LHC Effective Model for Optics Corrections

Maël Le Garrec

CERN, April 25, 2024

Temporary Plan

- b5 studies
  - DA simulations
    * Knobs created via resp matrix
    * Knobs tested via MADX with rdt tunes
    * Same knob re-tested with OP tunes
    * How is DA computed?

Check yourself before you Shrek yourself.

ICE CUBE FT. SHREK

Abstract

Zusammenfassung

Acknowledgements

cimer les bros href et bonswouar

Contents

Glossary

Nomenclature

AC-Dipole Dipole magnet generating a variable oscillating field. Used to force beam oscillations for optics measurements. .

Aperture Maximum physical transverse size the beam can take in the accelerator without suffering losses.

ATS Factor Equivalent to the ratio of the virgin β-function to the β-function used in the current ATS scheme, at the edge of the arc.

Beta-function Variable of the twiss-parameters: β as a function of the longitudinal position s. Related to the transverse beam size: $\sigma(s) = \sqrt{\epsilon \cdot \beta(s)}$.

BPM Beam Position Monitor, gives the transverse position of the beam.

Chromaticity Tune change with momentum offset. Usually denoted as three orders: Q', Q'' and Q'''.

Coupling Correlation between the motion of particles in horizontal or vertical plane to the other. Strong coupling negatively impacts the optics and is usually avoided. .

Crosstalk Interferences between two electronic circuits.

Dipole Magnets with two poles, responsible for bending the particles in the accelerator..

Dispersion Change of orbit with momentum offset, mainly in the horizontal plane, created by the dipoles.

DOROS Low noise BPM. Currently can't be used with other BPMs due to synchronization issues.

Dynamic Aperture Maximum stable aperture. Above that size, the particles become unstable and become lost.

Emittance (ϵ) Unit describing the beam in phase space. A low emittance indicates a beam with a small momentum offset and confined to a small distance.

Laundau Octupole Octupoles that introduce a spread in the beam, making it more stable.

LBDS LHC Beam Dump System.

Orbit Feedback System responsible for acquisition and correction of the orbit.

Rigid Waist Shift Doing a waist shift by powering all the triplets at once. No individual trim.

Waist Location where the β-function is at is minimum in an IP. β^* refers to β_{waist}.

Waist Shift Changing the waist to have $\beta^* = \beta_{IP}$.

Acronyms

LHC Large Hadron Collider.

Symbols

action Action used as coordinate blabla.

1 Introduction

Contents

1.1. Motivation

1.2. Thesis Outline

1.3. Particle Accelerators and CERN

1.3.1. Particle Accelerators

GPT

The history of particle accelerators is a captivating narrative that spans over a century of scientific innovation and discovery. It is a journey that has fundamentally transformed our understanding of the universe's fundamental particles and their interactions. The concept of accelerating particles to high speeds originated in the late 19th century, with early experiments conducted by pioneers such as J.J. Thomson and Ernest Rutherford, who utilized basic devices like cathode ray tubes to propel electrons. One of the earliest breakthroughs in accelerator technology was the Cockcroft-Walton accelerator, introduced in 1932 by John Cockcroft and Ernest Walton. This pioneering device employed voltage multipliers to accelerate protons and ions, enabling the first artificial nuclear disintegration—a milestone that earned them the Nobel Prize in Physics in 1951. Building upon this achievement, the development of the synchrotron in the 1940s and 1950s by scientists like Edwin McMillan and Vladimir Veksler marked a significant stride. Synchrotrons harnessed magnetic fields to bend and accelerate charged particles in circular paths, advancing the study of particle properties. A key turning point emerged with the establishment of CERN (the European Organization for Nuclear Research) in 1954, which culminated in the creation of the Proton Synchrotron (PS) in 1959. This marked the emergence of a powerful era in accelerator science, enabling the discovery of novel particles and laying the groundwork for the formulation of the Standard Model of particle physics. Throughout the 1960s and 1970s, the advent of bubble chambers and bubble chamber detectors provided researchers with the ability to trace the paths of charged particles, leading to the revelation of various particles and their intricate interactions. Yet, the true marvel of accelerator technology came to the forefront with the construction of the Large Hadron Collider (LHC) at CERN, which commenced operation in 2008. The LHC, an awe-inspiring 27-kilometer ring of superconducting magnets, propels protons and heavy ions to velocities nearing the speed of light. The LHC's monumental achievement—the discovery of the Higgs boson in 2012—marked a crowning moment in particle physics, solidifying the vital role of particle accelerators in unraveling the fabric of the cosmos. As particle physicists peer into the future, the quest continues. Concepts such as linear colliders and advanced circular colliders are on the horizon, promising to delve even deeper into the enigmatic realm of fundamental particles and the forces that govern them. The history of particle accelerators underscores the profound human endeavor to explore the most intricate mysteries of the universe, revealing the intricate dance of particles that shape the cosmos and expanding the horizons of human knowledge.

1.3.2. The CERN Complex

GPT The CERN complex, located near Geneva, Switzerland, is a prominent center for particle physics research. Its centerpiece is the Large Hadron Collider (LHC), the world's largest particle accelerator with a 27-kilometer circumference. Here, protons and heavy ions are accelerated to near light speed and collide at various points for fundamental particle studies. Surrounding the LHC are significant particle detectors, including ATLAS, CMS, ALICE, and LHCb, designed to capture and analyze particles generated during these collisions. CERN also includes linear accelerators, the Proton Synchrotron (PS), Super Proton Synchrotron (SPS), and Antiproton Decelerator (AD), contributing to particle acceleration and antimatter research. Alongside these facilities, CERN houses the Theoretical Physics Department, where theorists collaborate with experimentalists. With research, administrative buildings, laboratories, and workshops, CERN provides a comprehensive environment for scientific exploration. Its history, including the 2012 discovery of the Higgs boson, underscores its importance in advancing particle physics and highlighting international scientific cooperation.

1.3.3. The Large Hadron Collider

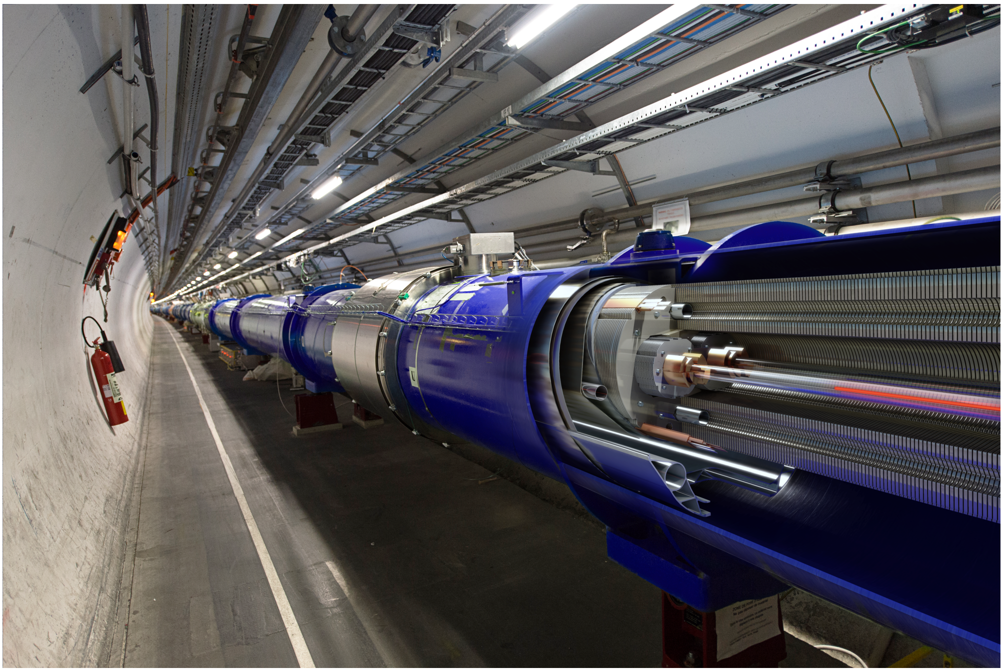

Figure 1.1.: 3D cut of a main LHC dipole [1].

speed of light, 11 000 turns per second, 12 000 amps in dipoles, number dipoles, price, parameters energy consumption, detectors and experiments, discoveries, collimators, optics, magnets, luminosity, arcs, IRs, schematics, cryostat, beta function FODO

1. Cycles & types of bunches: pilot for measurements

2

Concepts of Accelerator Physics

Contents

1. Dynamic Aperture
2. Luminosity

2

2.1. Introduction

2.2. Magnetic Fields

2.2.1. Nomenclature

Several notations coexist to denote magnetic fields. In this thesis, the *European Convention* [2] is used for field indices, as shown in Tab. 2.1. MAD-X, and MAD-NG, however, use the *American Convention*.

Multipole	MAD-X	Index	Normalized Strength
Dipole	0	1	K_1
Quadrupole	1	2	K_2
Sextupole	2	3	K_3
Octupole	3	4	K_4
Decapole	4	5	K_5
Dodecapole	5	6	K_6
Decatetrapole	6	7	K_7

Table 2.1.: Relation between field indices and multipoles.

As such, unless explicitly stated, quantities such as the magnetic strength b and normalized strength K will be expressed with this notation.

2.2.2. Multipole Expansion

2

A 2 dimension magnetic field in the planes x and y can be described as a sum of the normal and skew field gradients $\mathcal{B}$ and $\mathcal{A}$ with multipoles of order n, given by [3]:

$$B_y + iB_x = \sum_{n=1}^{\infty} (\mathcal{B}_n + i\mathcal{A}_n)\,(x+iy)^{n-1} \tag{2.1}$$

An ideal magnet would produce either a sole normal or skew field. However, this is not applicable to real-life magnets that are imperfect, due to design and manufacturing constraints. Field errors are thus introduced, relative to the main field of the ideal 2N-pole magnet at a reference radius r_{ref} [2], as shown in Eq. (2.2). The coefficients of the normal and skew relative field errors, referred to as a_n and b_n, are dimensionless but often given in *units* of 10^{-4}.

$$B_y + iB_x = \begin{cases} \mathcal{B}_N \cdot \sum_{n+1}^{\infty} (b_n + ia_n) \left(\frac{x+iy}{r_{ref}}\right)^{n-1}, \text{for normal magnets} \\ \mathcal{A}_N \cdot \sum_{n+1}^{\infty} (b_n + ia_n) \left(\frac{x+iy}{r_{ref}}\right)^{n-1}, \text{for skew magnets} \end{cases} \tag{2.2}$$

The normal and skew field components of order n for an imperfect 2N-pole magnet is thus given by the following equation:

$$\begin{aligned} \mathcal{B}_n &= \mathcal{B}_N \cdot \frac{b_n}{r_{ref}^{n-1}}, \\ \mathcal{A}_n &= \mathcal{A}_N \cdot \frac{a_n}{r_{ref}^{n-1}}. \end{aligned} \tag{2.3}$$

The unit of the field is relative to the multipole order n: $[\mathrm{Tm}^{1-n}]$.

2

2.2.3. Beam Rigidity and Normalization

Beam Rigidity

The beam rigidity refers to the resistance of a particle moving through the accelerator to the bending applied by the magnetic fields. It is derived from the Laurentz force [2] and relates the magnetic field B, the radius of curvature ρ to the momentum p and charge q of the particle:

$$B\rho = \frac{p}{q} \tag{2.4}$$

It is of interest when designing an accelerator to set the maximum field as well as the required radius of curvature for a specific momentum and particle. An interesting metric of an accelerator is also its *filling factor*, or percentage of dipoles in the machine. It can be calculated via the radius of curvature: $f = \rho/r$. A low filling factors means more space for other magnets, collimators, beam instrumentation, etc.

Field Normalization

The Beam Rigidity is also used as a way to normalize magnetic field strengths in particle accelerators where the momentum of the particle changes (i.e. acceleration). Normalized Normal and Skew components K_n and J_n are given by [3]:

$$\begin{aligned} K_n &= \frac{q}{p}(n-1)!\mathcal{B}_n, \\ J_n &= \frac{q}{p}(n-1)!\mathcal{A}_n. \end{aligned} \tag{2.5}$$

2.2.4. Hamiltonian Dynamics

The Hamiltonian describing the motion for the transverse planes of a given multipole or order n is given by [4–6]:

$$
\begin{aligned}
H &= \frac{q}{p}\Re\left[\sum_{n>1}(\mathcal{B}_n + i\mathcal{A}_n)\frac{(x+iy)^n}{n}\right] \\
&= \Re\left[\sum_{n>1}(K_n + iJ_n)\frac{(x+iy)^n}{n!}\right].
\end{aligned} \tag{2.6}
$$

Quite often, when studying the effect of a magnet on the beam, only one component is required, and the sum can thus be dropped. The normal and skew fields can also be isolated in order to consider their effect only:

$$
\begin{aligned}
N_n &= \frac{1}{n!}K_n\Re\left[(x+iy)^n\right] \\
S_n &= -\frac{1}{n!}J_n\Im\left[(x+iy)^n\right].
\end{aligned} \tag{2.7}
$$

2.3. Coordinate Systems

In circular accelerators, particle dynamics are represented using a traveling coordinate system. A reference orbit is determined by the lattice and its magnet strengths, forming the *optics*. In the case of a synchrotron, like the LHC, where the particles return to their original location after some turns, the reference orbit is also called the closed orbit.

2.3.1. Frenet-Serret System

The Frenet-Serret coordinate system moves along the ring on the reference orbit. The coordinates are then transverse: x and y, and longitudinal in the direction of travel: s. Figure 2.1 shows those coordinates.

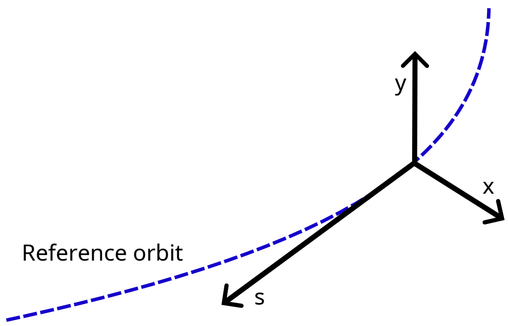

Figure 2.1.: Frenet-Serret coordinate system, commonly used in accelerator physics. The system moves along the reference orbit.

This coordinate system is widely used to simply describe a either an element's or a particle's position in the accelerator. Without any explicit mention, those are coordinates used in this thesis. It is frequent to use the variable z to refer to either x or y in equations.

2.3.2. Linear Lattice

Courant-Snyder Parameters

A circular accelerator is composed of many multipoles of different orders. A basic design only requires dipoles and quadrupoles in order to operate. Dipoles are used to bend the particles in order to form the ring, whereas quadrupoles are used to focus the beam to a focal point, similar to light optics. Those elements can be arranged in a particular order, to form a FoDo cell. Such cells present an alternating placement of focusing an defocusing quadrupoles with dipoles in between, as shown in Fig.2.2, and are usually repeated many times along the ring.

A lattice composed of only dipoles and quadrupoles, is referred to as a *linear* lattice. In a synchrotron, a circular particle accelerator, particles undergo transverse and longitudinal oscillations. As such, particles do not go back to their initial

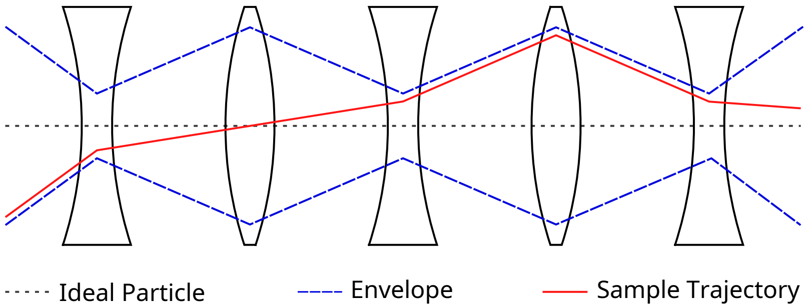

Figure 2.2.: Line composed of FoDo cells, a basic cell present in most accelerators, composed of a Focusing and a Defocusing quadrupole. The envelope is a factor of the β-function and the action J.

position before a certain number of turns. Taking into account those oscillations, the phase-space ellipse of a particle at a position s in the ring can be described with a new system: the Courant-Snyder parameters, also know as Twiss parameters or the *optics functions* [7], as shown in Fig. 2.3.

J, the action, an invariant of motion at a given energy, is related to the other quantities by:

$$J_z = \frac{1}{2}(\gamma_z \cdot z^2 + 2\alpha_z p_z \cdot z + \beta_z p_z^2). \tag{2.8}$$

The action can be related to the area in phase space, called the emittance: $\epsilon = 2J$. As the β parameter varies along the ring, it is referred to as the β-function and is related to the amplitude of the oscillations. Thus, the smaller is the β-function, the smaller is also the envelope of the beam. The number of oscillations per turn is called the *tune*, and is closely related to the β-function:

$$Q_{x,y} = \frac{1}{2\pi} \oint \frac{1}{\beta_{x,y}(s)} \mathrm{d}s. \tag{2.9}$$

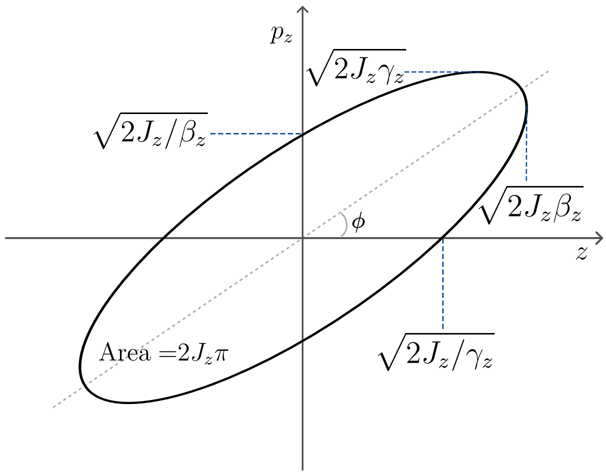

Figure 2.3.: Phase-space ellipse of a linear machine, parametrized by the Courant-Snyder parameters α, β and γ.

It is common to express the position of a particle using *action-angle* variables, allowing to switch between the Courant-Snyder parameters and the Frenet-Serret system:

$$\begin{aligned} z &= \sqrt{2J_z\beta_z}\cos\phi_z \\ p_z &= -\sqrt{\frac{2J_z}{\beta_z}}\left(sin\phi_z + \alpha_z\cos\phi_z\right). \end{aligned} \tag{2.10}$$

Normalized Coordinates

In order to simplify the description of the linear motion in a ring, a transformation can be applied to the previously seen coordinates. Figure Fig. 2.4 shows a phase-space described in both coordinates. The new coordinates, $\hat{z}$, and $\hat{p}_z$, are then expressed as factors of the α and β functions:

$$\begin{pmatrix} \hat{z} \\ \hat{p}_z \end{pmatrix} = \begin{pmatrix} \frac{1}{\sqrt{\beta_z}} & 0 \\ \frac{\alpha_z}{\sqrt{\beta_z}} & \sqrt{\beta_z} \end{pmatrix} \begin{pmatrix} z \\ p_z \end{pmatrix}. \tag{2.11}$$

This allows to describe the motion as a simple rotation, the new coordinates being only dependent on the invariant J_z and the phase ϕ_z:

$$\begin{aligned} \hat{z} &= \sqrt{2J_z} \cos\left(\phi_z\right), \\ \hat{p}_z &= \sqrt{2J_z} \cos\left(\phi_z\right). \end{aligned} \tag{2.12}$$

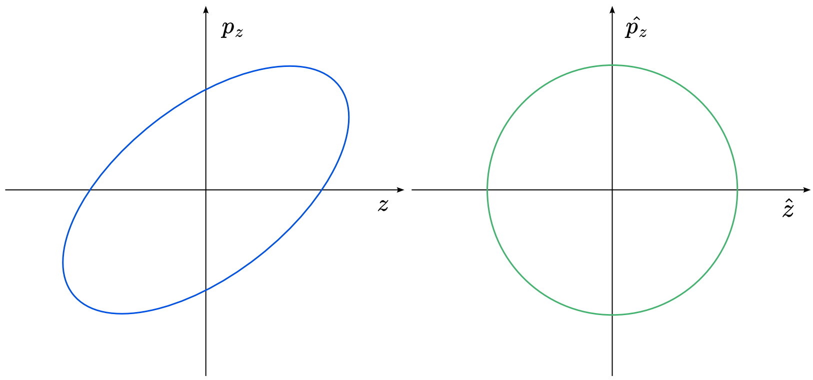

Figure 2.4.: Phase space described in both regular and normalized coordinates

Linear Transfer Maps

It is possible to describe the final position of a particle after going through an element via *transfer maps*. In linear optics, such linear maps are matrices. Those maps are symplectic, meaning they preserve the phase-space area. For a matrix $\mathcal{M}$ and positions z at the initial location and s, the general formula reads [8]:

2

$$\begin{pmatrix} z \\ z' \end{pmatrix}_s = M \cdot \begin{pmatrix} z \\ z' \end{pmatrix}_0 \tag{2.13}$$

This formalism assumes that the magnetic field is constant along the element in the longitudinal direction. Basic elements such as drifts, dipoles, quadrupoles can then be described be a simple 2×2 matrix:

$$M_{drift} = \begin{pmatrix} 1 & L \\ 0 & 1 \end{pmatrix}, \tag{2.14}$$

$$M_{dipole} = \begin{pmatrix} \cos(L/\rho) & \rho \sin(L/\rho) \\ -1/\rho \sin(L/\rho) & \cos(L/\rho) \end{pmatrix}, \tag{2.15}$$

$$M_{focusing\ quad.} = \begin{pmatrix} \cos\left(\sqrt{k_2}L\right) & 1/\sqrt{k_2}\sin\left(\sqrt{k_2}L\right) \\ -\sqrt{k_2}\sin\left(\sqrt{k_2}L\right) & \cos\left(\sqrt{k_2}L\right) \end{pmatrix}, \tag{2.16}$$

$$M_{defocusing\ quad.} = \begin{pmatrix} cosh\left(\sqrt{|k_2|}L\right) & 1/\sqrt{|k_2|}sinh\left(\sqrt{|k_2|}L\right) \\ \sqrt{|k_2|}sinh\left(\sqrt{|k_2|}L\right) & cosh\left(\sqrt{|k_2|}L\right) \end{pmatrix}, \tag{2.17}$$

where L is the length of the element, ρ the radius of curvature of the orbit and k_2 the normalized strength of quadrupoles. In the case of quadrupoles, a focusing matrix should be used in the horizontal plane for focusing quadrupoles, where defocusing matrices should be used in the vertical plane. The opposite goes for defocusing quadrupoles.

Transfer matrices can be combined together to describe a larger group of elements, as the FoDo cell seen previously. Its transfer matrix can then be expressed as:

$$M_{FoDo} = M_{focusing\ quad} \cdot M_{drift} \cdot M_{defocusing\ quad} \cdot M_{drift}. \tag{2.18}$$

For a closed machine, a full revolution can be described by a so-called *one-turn* *map*, being the transfer matrix of the whole machine, denoted $\mathcal{M}$. Such a map can potentially contain thousands of elements.

Symplecticity An important property of any transformation is that they need to be symplectic. A symplectic transformation preserves the volume in phase space.

2.3.3. Non-Linear Lattice

So far, Courant-Snyder parameters were a good way to describe the distribution of positions and velocities of particles in the transverse plane. One caveat of using this formalism is that it is restrained to linear optics and does not describe non-linear beam dynamics such as resonances or the effects arising from an arrangement of several multipoles together.

Lie Algebra

One way to describe non-linear effects is to introduce Lie Algebra [9], a powerful algebra able to describe transformations, symmetries and their associated conserved quantities.

The Lie algebra is a vector space, denoted $\mathfrak{g}$, equipped with a binary operation called the *Lie bracket* and denoted $[x, y]$ for two vectors x and y. Any vector space equipped with a Lie bracket (or commutator) satisfying the following conditions is called a Lie algebra:

- Bilinearity:

$$\begin{aligned} [ax + by, z] &= a[x, z] + b[y, z], \\ [z, ax + by] &= a[z, x] + b[z, y], \quad \forall x, y, z \in \mathfrak{g} \text{ and } a, b \text{ scalars} \end{aligned} \tag{2.19}$$

- Alternativity:

$$[x, x] = 0, \quad \forall x \in \mathfrak{g} \tag{2.20}$$

- Anticommutativity:

$$[x, y] = -[y, x], \quad \forall x, y \in \mathfrak{g} \tag{2.21}$$

- The Jacobi identity:

$$[x, [y, z]] + [y, [z, x]] + [z, [x, y]] = 0, \quad \forall x, y, z \in \mathfrak{g} \tag{2.22}$$

The *Lie bracket*, plays a central role in the Lie algebra. It describes how dynamical variables evolve under infinitesimal symplectic transformations.

Poisson Brackets

To create a Lie algebra, an operation satisfying the previous conditions needs to be found. In accelerator physics, *Poisson brackets* are chosen [9, 10]. Poisson brackets are used to describe continuous symmetries, conserved quantities, and the evolution of the dynamical variables in the system.

Let's consider position and momentum coordinates $q_i \cdots q_n$ and $p_i \cdots p_n$ of a 2n-dimensional phase space. Usually, those would be x, y, p_x and p_y for transverse coordinates. The Poisson brackets of two functions f and g is then defined by:

$$[f, g] = \sum_{i=1}^{n} \frac{\partial f}{\partial q_i}\frac{\partial g}{\partial p_i} - \frac{\partial f}{\partial p_i}\frac{\partial g}{\partial q_i}. \tag{2.23}$$

The evolution of coordinates and momenta in time is described by Hamilton's equations of motion, which can be naturally expressed with Poisson brackets:

$$\begin{aligned} \frac{\mathrm{d}q_i}{\mathrm{d}t} &= \frac{\partial H}{\partial p_i} = [q_i, H] \\ \frac{\mathrm{d}p_i}{\mathrm{d}t} &= -\frac{\partial H}{\partial q_i} = [p_i, H]. \end{aligned} \tag{2.24}$$

2

Lie Operator

Given a function f, a differential operator called *Lie operator* is defined, and is closely related to the previously seen Poisson bracket:

$$:f:=\sum_{i=1}^{n}\frac{\partial f}{\partial q_i}\frac{\partial}{\partial p_i}-\frac{\partial f}{\partial p_i}\frac{\partial}{\partial q_i}. \tag{2.25}$$

The action of this operator on a function g is equivalent to the Poisson brackets, as in:

$$:f:g=[f,g]. \tag{2.26}$$

A particular power series of this Lie operator can now be defined, called *Lie transformation*:

$$\begin{aligned} e^{:f:}g &= \sum_{l=0}^{\infty}\frac{1}{l!}:f:^{l}g \\ &= g+[f,g]+\frac{1}{2!}[f,[f,g]]+\cdots. \end{aligned} \tag{2.27}$$

Non-Linear Transfer Maps

As introduced in 2.3.2, the dynamics of a particle beam in a circular accelerator can be described by *transfer maps*. A symplectic *One Turn Map* $\mathcal{M}$ that includes N non-linear elements is defined [9] as:

$$\mathcal{M}=e^{:h_N:}\cdot e^{:h_{N-1}:}\cdots e^{:h_1:}\cdot\mathcal{R} \tag{2.28}$$

where $\mathcal{R}$ is a matrix describing the linear motion over one turn and the h_i terms representing the Hamiltonian of each non-linear elements of the machine. Via the

Baker-Campbell-Hausdorff (BCH) theorem [11], previous Lie transformations can be combined and simplified:

$$e^{:h_1:} \cdot e^{:h_2:} = e^{:h:} \tag{2.29}$$

with

$$\begin{aligned} h =& h_1 + h_2 && \Rightarrow 1^{\text{st}} \text{ order} \\ &+ \frac{1}{2}[h_1, h_2] && \Rightarrow 2^{\text{ nd}} \text{ order} \\ &+ \frac{1}{12}[h_1, [h_1, h_2]] - \frac{1}{12}[h_2, [h_1, h_2]] && \Rightarrow 3^{\text{rd}} \text{ order} \\ &+ \cdots . \end{aligned} \tag{2.30}$$

The one turn map is thus expressed as a single Lie transformation:

$$\mathcal{M} = e^{:h:} \cdot \mathcal{R}. \tag{2.31}$$

In most cases, were the non-linear perturbations are small, the above series converges quickly and only the two first terms of Eq. (2.30) are used [12]. The resulting expression is then more elegant, being a simple sum of the Hamiltonians of the N non-linear elements:

$$\mathcal{M} = e^{:h_1+h_2+\cdots+h_N:} \cdot \mathcal{R}. \tag{2.32}$$

It is though to be noted that in this thesis experimental measurements show the evidence of higher order contributions. In order to fully understand the combined effect of multipoles, the BCH expansion needs to be expended further than the first two terms.

something about -L:H:

2

Normal Form

As non-linearities are introduced in the machine, the phase-space becomes distorted, resulting in J_z no longer being an invariant of motion. The previously seen normalization does not work anymore and the phase-space is no longer a simple circle. A new normalization is then introduced, called the *normal form*, with complex coordinates ζ, depending on new action and angle coordinates I_z and ψ_z:

$$\zeta_{z,\pm} = \sqrt{2I_z}e^{\mp i\psi_z}. \tag{2.33}$$

An exaggerated vision of such a phase-space in Courant-Snyder, normalized, and normal form coordinates can be seen in Fig. 2.5.

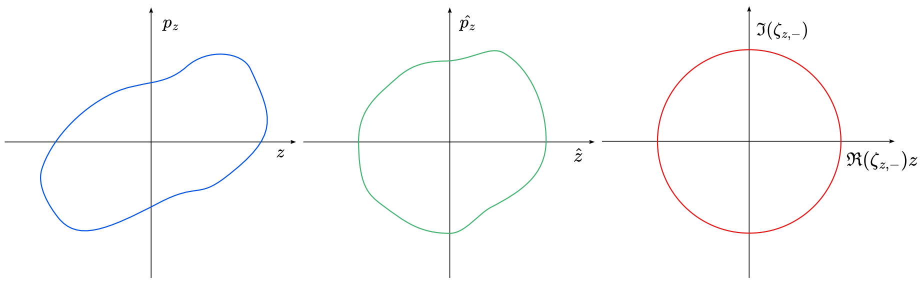

Figure 2.5.: Exaggerated phase space distorted by non-linearities described in regular, normalized and normal form coordinates.

The map defined previously in Eq. (2.31) can be rewritten in order to retrieve an invariant of motion I_z by introducing a generating function F:

$$\tilde{\mathcal{M}} = e^{:-F:}\mathcal{M}e^{:F:} \tag{2.34}$$

Such a generating function includes all the non-linearities, simplifying the calculations. Going back and forth from normalized to normal forms coordinates is then straightforward, as depicted in Fig. 2.6. The hamiltonian H is now only dependent on the action I_z.

$$\begin{tikzcd}
(\hat{z} \pm i\hat{p}_z)_N \arrow[r, "\hat{\mathcal{M}}"] \arrow[d, "e^{:-F:}"'] & (\hat{z} \pm i\hat{p}_z)_{N+1} \\
\zeta_N \arrow[r, "e^{:H:} \cdot \mathcal{R}"'] & \zeta_{N+1} \arrow[u, "e^{:F:}"']
\end{tikzcd}$$

Figure 2.6.: A one turn map from turn N to N+1 solved using a generating function F, transforming to normal form coordinates ζ, applying the linear rotation R and transforming back to normalized coordinates.

The function F is defined as

$$F = \sum_{jklm} f_{jklm} \zeta_{x,+}^{j} \zeta_{x,-}^{k} \zeta_{y,+}^{l} \zeta_{y,-}^{m}, \tag{2.35}$$

where f_{jklm} are the so-called Resonance Driving Terms (RDTs). The summation $jklm$ is done over all the combinations of j, k, l and m with $j + k + l + m = n$ for a multipole of order n, as shown in Eq. (2.36):

$$\sum_{jklm} = \sum_{j=0}^{n} \sum_{k=0}^{n} \sum_{l=0}^{n} \sum_{m=0}^{n} \quad ; \quad j + k + l + m = n. \tag{2.36}$$

The expression of the resonance driving terms is given by the global hamiltonian term h_jklm by

$$f_{jklm} = \frac{h_{jklm}}{1 - e^{i2\pi\left[(j-k)Q_x + (l-m)Q_y\right]}}, \tag{2.37}$$

2

where this coefficient is a summation over the hamiltonian terms of elements w in the lattice,

$$h_{jklm} = \sum_{w} h_{w,jklm} e^{i[(j-k)\Delta\phi_x + (l-m)\Delta\phi_y]}. \tag{2.38}$$

The expression of $h_{w,jklm}$ is itself derived from the general hamiltonian of Eq. (2.6) by applying a binomial expansion on the coordinates [6] as shows Eq. (2.39). Derivations and more information on resonance driving terms can be found in Appendix D.

$$h_{w,jklm} = -\Re\left[\frac{K_{w,n} + iJ_{w,n}}{j!k!l!m!2^{j+k+l+m}} i^{l+m} \beta_{w,x}^{\frac{j+k}{2}} \beta_{w,y}^{\frac{l+m}{2}}\right] \tag{2.39}$$

Transforming from the normal form coordinates back to the original normalized coordinates can be done using the right side of Fig. 2.6. Which is written, to second order, as:

$$\begin{aligned} h_z^{\pm} &= e^{:F:} \cdot \zeta_z^{\pm} \\ &\simeq \zeta_z^{\pm} + \left[F, \zeta_z^{\pm}\right] + \frac{1}{2!}\left[F, \left[F, \zeta_z^{\pm}\right]\right]. \end{aligned} \tag{2.40}$$

Using this equation to the first order and Eq. (2.33), the normalized coordinates can be expressed after N turns in Eq. (2.41).

$$\begin{aligned} (x - ip_x)(N) = &\sqrt{2I_x} e^{i\left(2\pi Q_x N + \psi_{x0}\right)} - \\ &2i \sum_{jklm} j f_{jklm} \left(2I_x\right)^{\frac{j+k-1}{2}} \left(2I_y\right)^{\frac{l+m}{2}} e^{i\left[(1-j+k)\left(2\pi Q_x N + \psi_{x0}\right) + (m-l)\left(2\pi Q_y N - \psi_{y0}\right)\right]} \\ (y - ip_y)(N) = &\sqrt{2I_y} e^{i\left(2\pi Q_y N + \psi_{y0}\right)} - \\ &2i \sum_{jklm} l f_{jklm} \left(2I_x\right)^{\frac{j+k}{2}} \left(2I_y\right)^{\frac{l+m-1}{2}} e^{i\left[(k-j)\left(2\pi Q_x N + \psi_{x0}\right) + (1-l+m)\left(2\pi Q_y N - \psi_{y0}\right)\right]}. \end{aligned} \tag{2.41}$$

It is to be observed that some f_{jklm} terms will not contribute to the motion of the particle in a given plane due to the dependence on j or l.

2.4. Examples of Maps

It is important to remember that two expansions are used when creating non linear transfer maps. When referring to the order of a map, it is the order of the BCH formula, used to combine Hamiltonians, that is referred to. The Lie transformation to transport the coordinates themselves is usually only taken to the first order.

2.4.1. Non-Linear Transfer of a Single Sextupole

Here, we are interested on the effect of a single sextupole on the regular frenet-serret coordinates x, y, p_x and p_y. Let's consider a sextupole with strength K_3 and a normal field,

$$H_3 = \frac{1}{6}K_3(x^3 - 3xy^2). \tag{2.42}$$

A transfer map, from longitudinal coordinate s_0 to s_1, consisting of only this element is the following:

$$\begin{pmatrix} x \\ p_x \\ y \\ p_y \end{pmatrix}_{s_1} = e^{L:H_3:} \begin{pmatrix} x \\ p_x \\ y \\ p_y \end{pmatrix}_{s_0}, \tag{2.43}$$

where L is the length of the multipole. Using Eq. (2.27) to expand the Lie transformation to the first order, it can be rewritten as

$$\begin{aligned} e^{L:H_3:}x &= x + [L \cdot H_3, x], \\ e^{L:H_3:}p_x &= p_x + [L \cdot H_3, p_x], \\ e^{L:H_3:}y &= y + [L \cdot H_3, y], \\ e^{L:H_3:}p_y &= p_y + [L \cdot H_3, p_y]. \end{aligned} \tag{2.44}$$

Applying the poisson bracket of Eq. (2.23) on x or y yields 0, as neither the Hamiltonian nor x and y are dependent on p_x and p_y.

$$\begin{aligned} [L \cdot H_3, x] &= \overbrace{\frac{\partial(L \cdot N_3)}{\partial x}\frac{\partial x}{\partial p_x}}^{0} - \overbrace{\frac{\partial(L \cdot N_3)}{\partial p_x}\frac{\partial x}{\partial x}}^{0} + \underbrace{\frac{\partial(L \cdot N_3)}{\partial y}\frac{\partial x}{\partial p_y}}_{0} - \underbrace{\frac{\partial(L \cdot N_3)}{\partial p_y}\frac{\partial x}{\partial y}}_{0} \\ &= 0. \end{aligned} \tag{2.45}$$

The poisson bracket applied on p_x or p_y though evaluates to a non-zero value, as the momentum is present in $p_{x,y}$ while x, y are present in the Hamiltonian:

$$\begin{aligned} [L \cdot H_3, p_x] &= \frac{\partial(L \cdot N_3)}{\partial x}\frac{\partial p_x}{\partial p_x} - \overbrace{\frac{\partial(L \cdot N_3)}{\partial p_x}\frac{\partial p_x}{\partial x}}^{0} + \underbrace{\frac{\partial(L \cdot N_3)}{\partial y}\frac{\partial p_x}{\partial p_y}}_{0} - \underbrace{\frac{\partial(L \cdot N_3)}{\partial p_y}\frac{\partial p_x}{\partial y}}_{0} \\ &= \frac{1}{2}K_3 L(x^2 - y^2) \end{aligned} \tag{2.46}$$

The same method is used for p_y. The final form of the transfer map Eq. (2.43) is then the following:

$$\begin{pmatrix} x \\ p_x \\ y \\ p_y \end{pmatrix}_{s_1} = \begin{pmatrix} 1 & & & \\ & \frac{1}{2}K_3L(x^2-y^2) & & \\ & & 1 & \\ & & & -K_3Lxy \end{pmatrix} \begin{pmatrix} x \\ p_x \\ y \\ p_y \end{pmatrix}_{s_0} . \tag{2.47}$$

It is not necessary to go higher than the first order, as the second order of the expansion of the Lie transformation is 0 ; p_x is indeed not present in the result of the first poisson bracket:

$$\begin{aligned} \frac{1}{2!}[L \cdot H_3, [L \cdot H_3, p_x]] &= \frac{1}{2!}\left[L\frac{1}{6}K_3(x^3-3xy^2), \left[L\frac{1}{6}K_3(x^3-3xy^2), p_x\right]\right] \\ &= \frac{1}{2!}\left[L\frac{1}{6}K_3(x^3-3xy^2), \frac{1}{2}K_3L(x^2-y^2)\right] \\ &= \frac{1}{2!} \cdot 0 \\ &= 0 \end{aligned} \tag{2.48}$$

2.4.2. Non-Linear Transfer of Two Sextupoles

We saw previously that a single sextupole only acts as a sextupole when it is alone in the transfer map, which is expected. Let's now consider two sextupoles which hamiltonians are denoted H_1 and H_2.

Creating a map consisting of only two sextupoles does not make much sense, as it finally results in one sextupole as their coordinates are the same. Instead, a drift is added between the two elements. The Hamiltonian of a drift of length L_D is given by [13],

$$D = -\frac{L_D}{2}(p_x^2 + p_y^2). \tag{2.49}$$

The application of the lie transformation on the canonical coordinates is then very simple, as no higher orders arise ($[D, [D, x]] = 0$):

$$\begin{aligned} e^{:D:}x &= x + L_D p_x, \\ e^{:D:}p_x &= p_x. \end{aligned} \tag{2.50}$$

The transfer map of such a line is then the following,

$$\mathcal{M} = e^{:Z:} = e^{:H_2:} \cdot e^{D:H_1:}, \tag{2.51}$$

describing the evolution of coordinates from a longitudinal position s_0 to s_1,

$$\begin{pmatrix} x \\ p_x \\ y \\ p_y \end{pmatrix}_{s_1} = \mathcal{M} \cdot \begin{pmatrix} x \\ p_x \\ y \\ p_y \end{pmatrix}_{s_0} \tag{2.52}$$

In order to combine those elements, the BCH formula from Eq. (2.30) is used, presented here to the third order for two elements,

$$Z = \underbrace{H_2 + H_1}_{\text{First order}} + \underbrace{\frac{[H_2, H_1]}{2}}_{\text{Second order}} + \underbrace{\frac{[H_2, [H_2, H_1]]}{12} - \frac{[H_1, [H_2, H_1]]}{12}}_{\text{Third order}} \tag{2.53}$$

First Order To the first order, the resulting effective hamiltonian is only the summation of two sextupoles.

Second Order The drift added to change the coordinates of H_1 allows the poisson bracket to evaluate to a non-zero value. Octupolar-like terms indeed appear in the effective hamiltonian. From this, it can be inferred that two sextupoles will interact together and introduce effects like amplitude detuning, second order chromaticity and RDTs. Details of the derivation can be found in Appendix B.

Third Order To the third order, even higher orders such as decapolar-like effects appear. Such effects include the third order chromaticity, chromatic amplitude detuning and RDTs.

Remark It is to be noted that while sextupoles do introduce higher-order terms, these are typically small in comparison to those brought by the actual higher-order multipoles, making them thus often negligible.

2.5. Beam Observables

title?
Linear observables
Optics

2.5.1. Dispersion

Treating a beam as a single particle having the design momentum p_0 leads to a machine with no apparent ill effect related to that momentum. However, when considering a particle beam where each particle follows a distribution in momentum, a few effects arise from this deviation, called the *momentum offset*, δ. It is defined as a relative difference to the design momentum:

$$\delta = \frac{p - p_0}{p_0}. \tag{2.54}$$

Those effects are referred to as *chromatic aberrations*. The first and most important to consider is the *dispersion*. Dispersion results from a particle with a momentum offset being deflected differently by the dipoles compared to a particle at the design momentum. Figure 2.7 shows an example of deflection.

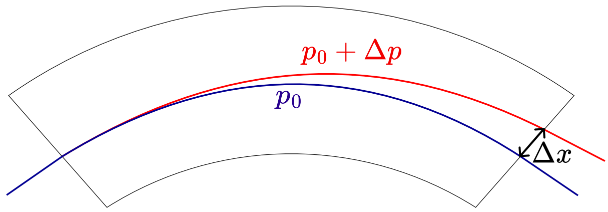

Figure 2.7.: Particles with a momentum offset will be deflected differently by dipoles. This offset in position can be described by the dispersion function.

The particle is still subject to the other properties of the lattice, but with a different orbit, described by Eq. (2.7).

$$\begin{aligned} D_x(s) &= \frac{\Delta x(s)}{\delta} \\ D_y(s) &= \frac{\Delta y(s)}{\delta} \end{aligned} \tag{2.55}$$

2.5.2. β-function

As seen previously in 2.3.2, the β-function is related to the amplitude of oscillations of the beam. Figure 2.8 shows how the β-function oscillates along the ring due to quadrupoles focusing and defocusing properties. The β-function is an important quantity found as a factor in several other observables that will be described later in this thesis.

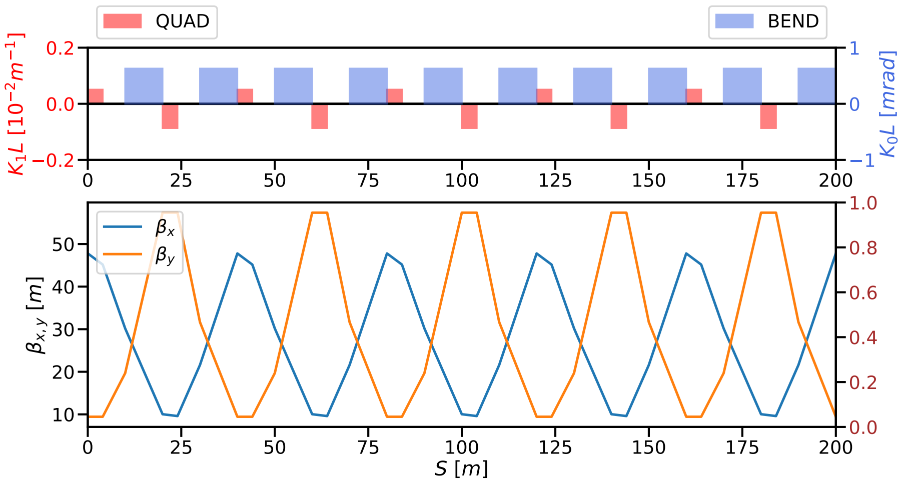

Figure 2.8.: Evolution of the β-function along the lattice. Horizontal and vertical beatings are usually opposite given the focusing and defocusing properties of quadrupoles in each plane.

A difference in β-function compared to the design leads to possible unstable and larger beams, degrading its properties and making it harder to control. The relative difference in β-function is called the beta-beating, expressed in percents:

$$\text{beating [\%]} = \frac{\beta_z(s) - \beta_z(s)_{model}}{\beta_z(s)_{model}}. \tag{2.56}$$

2.5.3. Coupling

In a perfect scenario, the particle motion of each transverse plane is independent, or *uncoupled*. In practice, this transverse motion can be altered by some magnetic elements, giving rise to *betatron coupling* where the motion of each plane is not independent anymore. Such elements can be quadrupoles, mounted with a roll error introducing skew-quadrupolar fields, which are the main source of coupling in the

2

LHC [14]. Field imperfections, solenoids and feed-down from higher orders can also contribute to coupling.

The resonances $Q_x + Q_y$ and $Q_x - Q_y$, called the *sum* and *difference* resonances, are mainly excited by skew quadrupoles. When coupling is present in the machine, the former may lead to unstable motion while the latter introduces an periodic exchange of emittance between the planes, keeping it stable. They can be characterized by the RDTs f_{1010} and f_{1001}.

Effects of normal multipoles start showing their skew counterpart (and vice versa) as the motion of transverse planes become coupled. This is demonstrated in Chapter 6 with skew-octupolar RDTs contributed to by normal octupoles in the presence of coupling.

2.5.4. Momentum Compaction Factor

2.6. Detuning Effects

blabla

2.6.1. Chromaticity

Chromaticity is the tune change ΔQ relative to the momentum offset δ. Chromaticity can be described by a Taylor expansion, given by

$$Q(\delta) = Q_0 + Q'\delta + \frac{1}{2!}Q''\delta^2 + \frac{1}{3!}Q'''\delta^3 + O(\delta^4). \tag{2.57}$$

Or, more generally, rewritten as a sum to include all orders up to n:

$$Q(\delta) = Q_0 + \sum_{i=1}^{n} \frac{1}{i!}Q^{(i)}\delta^i. \tag{2.58}$$

The first order of the chromaticity expansion, Q', is generally simply referred to as *chromaticity*, sometimes as *linear chromaticity*. The other terms are thus referred to as *non-linear chromaticity*.

The chromaticity change induced by a single element of order n and length L can be derived from the Hamiltonian of Eq. (2.6), averaging over the phase variables and differentiating relative to the actions $J_{x,y}$ and the momentum offset δ:

$$\Delta Q_{x,y}^{(n)} = \frac{\partial^n Q_{x,y}}{\partial^n \delta} = \frac{1}{2\pi} \int_L \left\langle \frac{\partial^{(n+1)} H}{\partial J_{x,y} \partial^n \delta} \right\rangle \mathrm{d}s. \tag{2.59}$$

Detailed derivations can be found in [15].

Natural Chromaticity from Quadrupoles In a purely linear lattice, the linear chromaticity, Q', is a result of the momentum dependence of the quadrupoles' focusing. It is in this case called the *natural chromaticity* and can be derived from the normal hamiltonian of Eq. (2.7) and expressing the normalized magnet strength K with a dependence on δ via P as $P_0(1+\delta)$:

$$K_n = \frac{q}{P_0} \frac{1}{1+\delta} (n-1)! B_n \tag{2.60}$$

The normal field of a quadrupole is then given by

$$\mathcal{N}_2(x,y) = \frac{1}{2} \frac{q}{P_0} \frac{1}{1+\delta} B_2 (x^2 - y^2) \tag{2.61}$$

By operating a variable change to the angle coordinates ($x \longrightarrow \sqrt{2J_x\beta_x}\cos\phi_x$ and $y \longrightarrow \sqrt{2J_y\beta_y}\cos\phi_y$), the following equation linking the β-function and δ to the normal field is obtained:

$$\mathcal{N}_2(x,y) = \frac{1}{2} \frac{q}{P_0} \frac{1}{1+\delta} B_2 \left[\left(\sqrt{2J_x\beta_x} \cos\phi_x \right)^2 - \left(\sqrt{2J_y\beta_y} \cos\phi_y \right)^2 \right]. \tag{2.62}$$

Following Eq. (2.59), the natural chromaticity Q' induced by quadrupoles is given by:

$$\begin{aligned} \Delta Q'_x &= \frac{1}{2\pi}\int_L \frac{\partial^2 \langle \mathcal{N}_2 \rangle}{\partial J_x \partial \delta}\,\mathrm{d}s \quad ; \quad & \Delta Q'_y &= \frac{1}{2\pi}\int_L \frac{\partial^2 \langle \mathcal{N}_2 \rangle}{\partial J_y \partial \delta}\,\mathrm{d}s \\ &= -\frac{1}{4\pi}\frac{q}{P_0}B_2 L \beta_x & &= \frac{1}{4\pi}\frac{q}{P_0}B_2 L \beta_y \end{aligned} \tag{2.63}$$

Linear Chromaticity from Sextupoles The first order chromaticity Q' is contributed to by sextupoles in the presence of off-momentum particles. The normal field of a sextupole, following Eq. (2.7) is given by

$$\mathcal{N}_3(x, y) = \frac{1}{3!}(x^3 - 3xy^2). \tag{2.64}$$

As the momentum offset δ introduces a change in orbit via dispersion [16], a variable change can be operated on both x and y, as shown in Eq. (2.65). In this thesis, vertical dispersion will be though neglected.

$$\begin{aligned} x &\longrightarrow x + \Delta x = x + D_x\delta \\ y &\longrightarrow y + \Delta y = y + D_y\delta \end{aligned} \tag{2.65}$$

The positions x and y can once be replaced, using the twiss parameters, giving the full expression:

$$
\begin{aligned}
\mathcal{N}_3(x+\Delta x, y) = \frac{1}{6}K_3\Big[& \left(\sqrt{2J_x\beta_x}\cos\phi_x\right)^3 \\
& + 3\left(\sqrt{2J_x\beta_x}\cos\phi_x\right)^2 D_x\delta \\
& + 3\left(\sqrt{2J_x\beta_x}\cos\phi_x\right) D_x^2\delta^2 \\
& + D_x^3\delta^3 \\
& - 3\left(\sqrt{2J_x\beta_x}\cos\phi_x\right)\left(\sqrt{2J_y\beta_y}\cos\phi_y\right)^2 \\
& - 3D_x\delta(\sqrt{2J_y\beta_y}\cos\phi_y)^2\Big]
\end{aligned}
\tag{2.66}
$$

Averaging over the phase variables removes any odd cosine:

$$
\begin{aligned}
\langle\mathcal{N}_3(x+\Delta x, y)\rangle = \frac{1}{6}K_3\Big(& 3J_x\beta_x D_x\delta \\
& + D_x^3\delta^3 \\
& - 3D_x\delta J_y\beta_y\Big)
\end{aligned}
\tag{2.67}
$$

The chromaticity can then obtained by differentiating relative to the action $J_{x,y}$ to obtain the tune, and then by the momentum offset δ.

$$
\begin{aligned}
\Delta Q'_x &= \frac{1}{2\pi}\int_L \frac{\partial^2\langle\mathcal{N}_3\rangle}{\partial J_x\partial\delta}\,\mathrm{d}s \quad ; \quad & \Delta Q'_y &= \frac{1}{2\pi}\int_L \frac{\partial^2\langle\mathcal{N}_3\rangle}{\partial J_y\partial\delta}\,\mathrm{d}s \\
&= \frac{1}{2\pi}L\frac{1}{2}K_3\beta_x D_x & &= -\frac{1}{2\pi}L\frac{1}{2}K_3\beta_y D_x \\
&= \frac{1}{4\pi}K_3 L\beta_x D_x & &= -\frac{1}{4\pi}K_3 L\beta_y D_x
\end{aligned}
\tag{2.68}
$$

From this last equation, it is apparent than sextupoles are not a source of chromaticity of higher orders in the presence of linear dispersion. In the presence of second order dispersion [16], sextupoles can generate some amount of Q'', usually negligible.

Non-Linear Chromaticity Higher orders of the chromaticity function are described in [15] and follow the same logic as for the linear chromaticity from sextupoles. A general formula can be found for the chromaticity of order $n, n > 2$:

$$\begin{aligned} \Delta Q_x^{(n)} &= \frac{1}{4\pi} K_{n+2} L \beta_x D_x^n \\ \Delta Q_y^{(n)} &= -\frac{1}{4\pi} K_{n+2} L \beta_x D_x^n \end{aligned} \tag{2.69}$$

2.6.2. Amplitude Detuning

Amplitude detuning is a tune shift induced by the amplitude of oscillations of a particle. This detuning is directly related to the emittance and can be described via a Taylor expansion around the emittance of both planes, ϵ_x and ϵ_y. Equation (2.70) shows this expansion up to the second order. Further expansions can be found in [15].

$$\begin{aligned} Q_z(\epsilon_x, \epsilon_y) = Q_{z0} &+ \left(\frac{\partial Q_z}{\partial \epsilon_x} \epsilon_x + \frac{\partial Q_z}{\partial \epsilon_y} \epsilon_y \right) \\ &+ \frac{1}{2!} \left(\frac{\partial^2 Q_z}{\partial \epsilon_x^2} \epsilon_x^2 + 2 \frac{\partial^2 Q_z}{\partial \epsilon_x \partial \epsilon_y} \epsilon_x \epsilon_y + \frac{\partial^2 Q_z}{\partial \epsilon_y^2} \epsilon_y^2 \right) + \dots \end{aligned} \tag{2.70}$$

The first order terms of amplitude detuning are generated by octupoles, and to some extent by sextupoles when considering their higher order contributions. Those higher contributions are usually measurable but small compared to the ones of normal octupoles. It is to be noted that each order does not correspond directly to a multipole order, like for chromaticity seen previously. While it is the case for the simple partial derivatives, the crossterms are instead generated by multipoles of higher orders. Further derivations can be found in Appendix C.

2.6.3. Chromatic Amplitude Detuning

Similar to amplitude detuning, *chromatic amplitude detuning* is a tune shift induced by the amplitude of oscillations of a particle but with an additional dependence on the momentum offset. This effect can be described by a Taylor expansion around the emittance of both planes ϵ_x, ϵ_y, and the momentum offset δ. Equation (2.71) shows this expansion up to the second order.

$$
\begin{aligned}
Q_z(\epsilon_x, \epsilon_y, \delta) = Q_{z0} &+ \left[\frac{\partial Q_z}{\partial \epsilon_x}\epsilon_x + \frac{\partial Q_z}{\partial \epsilon_y}\epsilon_y + \frac{\partial Q_z}{\partial \delta}\ \delta \right] \\
&+ \frac{1}{2!}\left[\frac{\partial^2 Q_z}{\partial \epsilon_x^2}\epsilon_x^2 + \frac{\partial^2 Q_z}{\partial \epsilon_y^2}\epsilon_y^2 + \frac{\partial^2 Q_z}{\partial \delta^2}\ \delta^2 \right. \\
&\qquad \left. + 2\frac{\partial^2 Q_z}{\partial \epsilon_x \partial \epsilon_y}\epsilon_x\epsilon_y + 2\frac{\partial^2 Q_z}{\partial \epsilon_x \partial \delta}\epsilon_x\delta + 2\frac{\partial^2 Q_z}{\partial \delta \partial \epsilon_y}\delta\epsilon_y \right] \\
&+ \ldots
\end{aligned}
\tag{2.71}
$$

Sextupolar contributions To the first order, the terms of the chromatic amplitude detuning are shared with the classic amplitude detuning, which are not contributed to by sextupoles. The last term however is the linear chromaticity, seen previously in 2.6.1.

Octupolar contributions Similar to the sextupolar contributions, to the first order, the terms are shared with amplitude detuning. The first terms $\frac{\partial Q_z}{\partial \epsilon_x}\epsilon_x$ and $\frac{\partial Q_z}{\partial \epsilon_y}\epsilon_y$ are then contributed to by octupoles. The second order chromaticity Q'' appears when expanding to the second order.

Decapolar contributions So far, only terms with amplitude detuning and chromaticity have been seen. The terms highlighted in orange, in Eq. (2.72), are the

2

terms contributed to by decapoles. Terms depending on both the emittance and the momentum offset are present, as well as the third order chromaticity Q'''.

$$
\begin{aligned}
Q_z(\epsilon_x, \epsilon_y, \delta) = Q_{z0} &+ \left[\frac{\partial Q_z}{\partial \epsilon_x}\epsilon_x + \frac{\partial Q_z}{\partial \epsilon_y}\epsilon_y + \frac{\partial Q_z}{\partial \delta}\delta\right] \\
&+ \frac{1}{2!}\left[\frac{\partial^2 Q_z}{\partial \epsilon_x^2}\epsilon_x^2 + \frac{\partial^2 Q_z}{\partial \epsilon_y^2}\epsilon_y^2 + \frac{\partial^2 Q_z}{\partial \delta^2}\delta^2\right. \\
&\qquad \left. + 2\frac{\partial^2 Q_z}{\partial \epsilon_x \partial \epsilon_y}\epsilon_x\epsilon_y + 2\frac{\partial^2 Q_z}{\partial \epsilon_x \partial \delta}\epsilon_x\delta + 2\frac{\partial^2 Q_z}{\partial \delta \partial \epsilon_y}\delta\epsilon_y\right] \\
&+ \frac{1}{3!}\left[\frac{\partial^3 Q_z}{\partial \delta^3}\delta^3 + \frac{\partial^3 Q_z}{\partial \epsilon_x^3}\epsilon_x^3 + \frac{\partial^3 Q_z}{\partial \epsilon_y^3}\epsilon_y^3 + \cdots\right]
\end{aligned}
\tag{2.72}
$$

Further derivations can be found in Appendix C.

2.7. Resonances

2.7.1. Tune Diagram

The resonances discussed in this thesis are related to the optics of the accelerator. Such resonances create unstable motion and can lead to loosing particles. Those perturbations arise from particles oscillating at frequencies excited by certain multipoles.

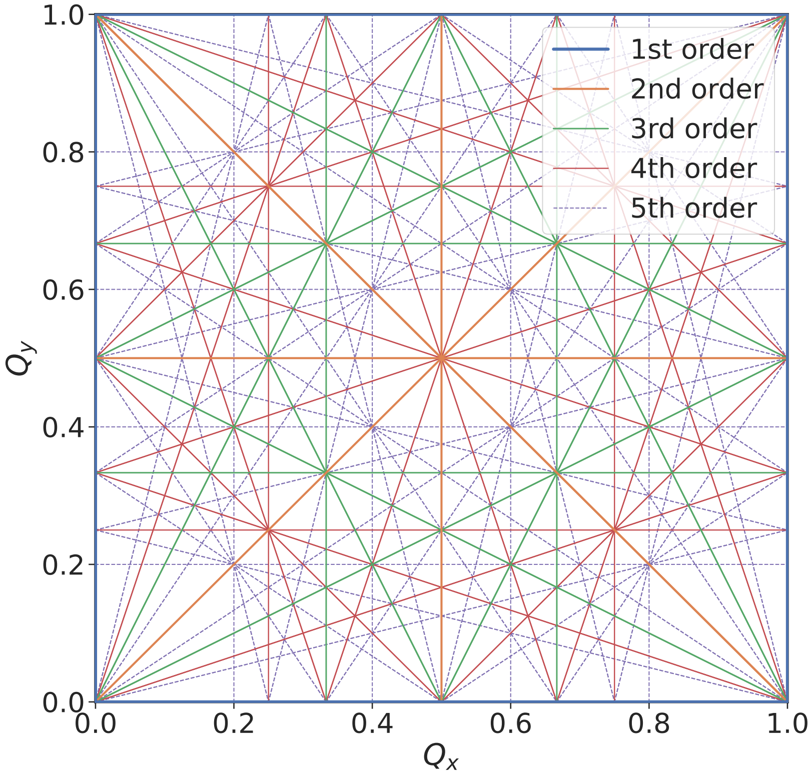

Figure 2.9.: Tune diagram with resonances lines excited by multipoles up to decapole ($n \leq 5$). The working point of the machine is chosen in an area where few lines are present.

Fig. 2.9 shows a tune diagram where the fractional part of tunes Q_x and Q_y can be related to resonance lines excited by multipoles up to decapoles ($n = 5$).

It becomes apparent that the diagram fills quickly when considering further orders, as shows Fig. 2.10. Thankfully, the higher the multipole order, the weaker the resonances are. This makes choosing a working point possible, even if some particles are hitting resonance lines.

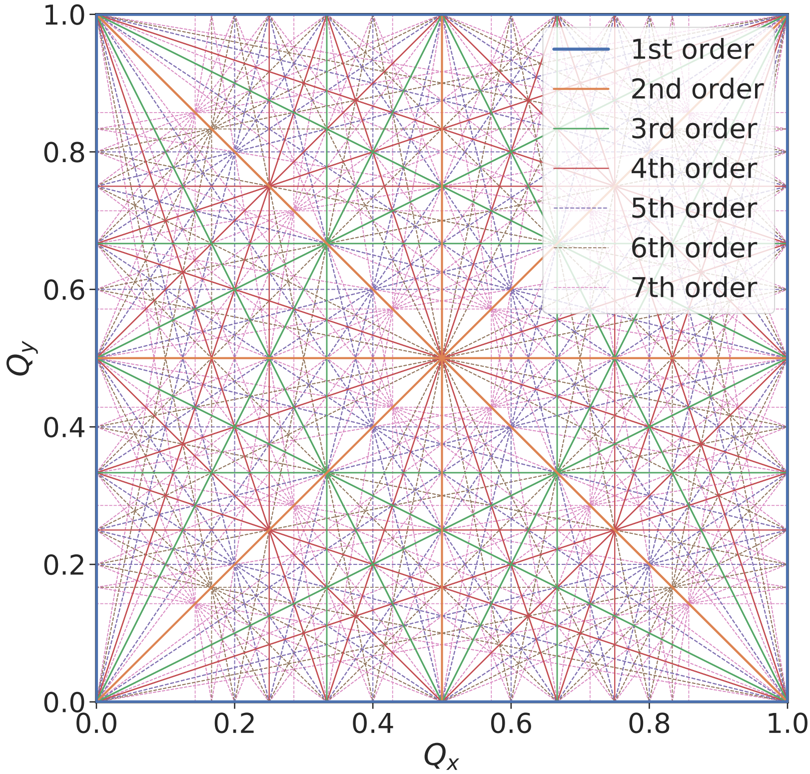

Figure 2.10.: Tune diagram with resonances lines excited by multipoles up to decatetrapole ($n \leq 7$). When considering higher orders, it becomes apparent that the beam will inevitably hit several resonances.

When considering the resonance driving terms f_{jklm} from Eq. (2.37), it can be noted that the term diverges for particular tune values. This leads to a disproportionate increase in particles position in phase-space, eventually leading to loosing them. Resonant conditions due to the tunes can thus be described by the following condition:

$$(j-k)Q_x + (l-m)Q_y = p \quad , \quad j,k,l,m,p \in \mathcal{Z}. \tag{2.73}$$

2.7.2. Frequency Spectrum

As seen in Eq. (2.41), resonance driving terms have an impact on the transverse position of a particle. This means that performing a FFT on such a signal will reveal spectral lines in the frequency spectrum. Each RDT f_{jklm} can thus be observed in either one or both frequency spectrums of transverse planes, at multiples of $Q_x \pm Q_y$. Eq. (2.74) shows where those lines would appear:

$$\begin{aligned} &H(1-j+k, m-l) && \text{horizontal line, if } j \neq 0 \\ &V(k-j, 1-l+m) && \text{vertical line, if } l \neq 0. \end{aligned} \tag{2.74}$$

The RDT f_{3000} coming from sextupoles can for example be seen in the horizontal spectrum at $(1-3+0)Q_x + (0-0)Q_y = -2Q_x$. For a value $Q_x = 0.27$, the line is seen at 0.46. in a spectrum bound in $[0, 0.5]$. No line can be seen in the vertical spectrum due to $l = 0$. Detailed tables of such lines for RDTs up to order 6 can be found in Appendix D.

The amplitude of each line will depend on the action I_z and the amplitude of the RDT [17]:

$$\begin{aligned} |H_{f_{jklm}}| &= 2j(2I_x)^{\frac{j+k-1}{2}}(2I_y)^{\frac{l+m}{2}}|f_{jklm}| \\ |V_{f_{jklm}}| &= 2l(2I_x)^{\frac{j+k}{2}}(2I_y)^{\frac{l+m-1}{2}}|f_{jklm}|. \end{aligned} \tag{2.75}$$

2.7.3. Resonance Driving Terms

By reworking the previous Eq. (2.75), it can be seen that RDTs are factors of the line amplitude and the actions I_x and I_z:

$$
\begin{aligned}
|f_{jklm}| &= \frac{|H_{f_{jklm}}|}{2j(2I_x)^{\frac{j+k-1}{2}}(2I_y)^{\frac{l+m}{2}}} \\
|f_{jklm}| &= \frac{|V_{f_{jklm}}|}{2l(2I_x)^{\frac{j+k}{2}}(2I_y)^{\frac{l+m-1}{2}}}.
\end{aligned}
\tag{2.76}
$$

In practice, an approximation of $J = I$ is done. The RDT is then the result of a fit of the line amplitude versus the action, as shown in Fig. 2.11.

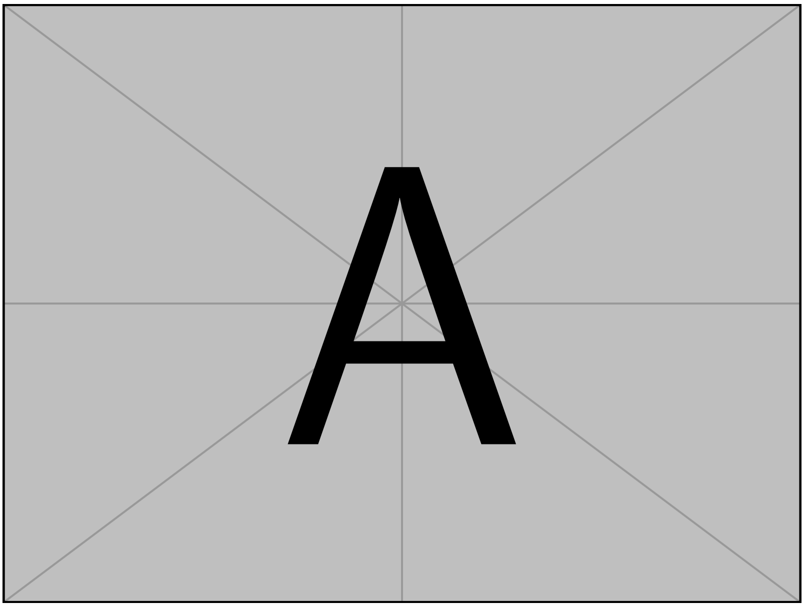

Figure 2.11.: .

3

Optics Measurements and Corrections

3

Contents

3.1. Beam Instrumentation

3.1.1. Beam Position Monitors

Beam Position Monitors (BPMs) are one of the most utilized and essential elements of beam diagnostics in particle accelerators. In the LHC, most of the BPMs are dual plane, and thus composed of four electrodes, distributed as two per plane. The BPM system consists of over than 550 BPMs pear beam, distributed along the ring, in the arcs and the IPs. The most common type, the *curved-button*, shown in Fig. 3.1a, is typically placed near quadrupoles [18].

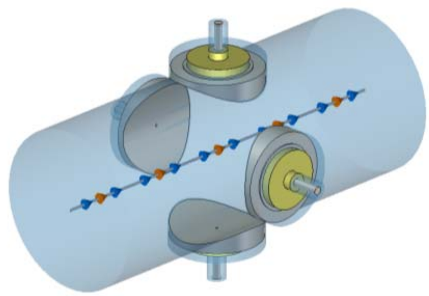

(a) Curved-button *"BPM"* type BPM of the LHC [18].

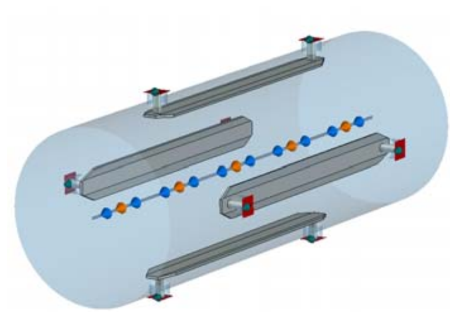

(b) Stripline *"BPMSW"* type BPM of the LHC [18].

Other pickups such as the *stripline*, shown in Fig. 3.1b, albeit more complex and expensive, offer a better signal to noise ratio and are capable of identifying the direction of the beam [18]. Such features are essential for the LHC, were both beams travel through the same aperture at the IPs.
The BPM response is not linear with the beam position, which requires a post-processing not systematically implemented in accelerators beam diagnostics systems. LHC's BPMs have been simulated and polynomials fitted to minimize this response error [19].

3.1.2. Beam Loss Monitors

Beam Loss Monitors are detectors mounted on various elements of the accelerator, such as magnets or collimators, to detect abnormal losses of particles. They play a crucial role in the protection of the machine, triggering a dump when losses exceed the threshold set for their respective element. BLMs use ionization chambers, working on the same principle as simple Geiger counters: a tube filled with gas, in presence of a high voltage.

Dashboards in the control room are regularly used to monitor the losses along the ring when performing optics measurements, as those prove to often be destructive.

3.1.3. AC-Dipole

The AC dipole of the LHC is a crucial component for optics studies. Its primary function is to excite the beam into large coherent oscillation, achieved by applying a sinusoidally oscillating dipole field [20]. By ramping up and down adiabatically the field, large coherent oscillations can be produced without any decoherence or emittance growth. Figure 3.2 shows an example of a measurement made with an AC-Dipole. Exciting the beam to large amplitudes make the study of linear optics, such as beta-beating easier, and that of non linear optics such as resonances possible.

The AC-Dipole is set to oscillate at a frequency Q_d, different from the natural tune of the machine Q and thus introduces systematic effects that needs to be compensated during the optics analysis. The new orbit of a particle under the influence of the AC-Dipole, at turn number n and observation point s, is given by [21]:

$$z(s,n) = \frac{BL}{4\pi\rho\delta_z} \cdot \sqrt{\beta_z(s)\beta_{z,0}} \cdot \cos\left(2\pi Q_{d,z}n + \phi_z(s) + \phi_{z,0}\right), \tag{3.1}$$

where B is the amplitude of the oscillating magnetic field, L the length of the AC-Dipole, $B\rho$ the magnetic rigidity, δ the difference between Q_d and Q, β and β_0 the beta function at the observed point and the AC-Dipole, ϕ and ϕ_0 the phase advance at the observed point and of the AC-Dipole.

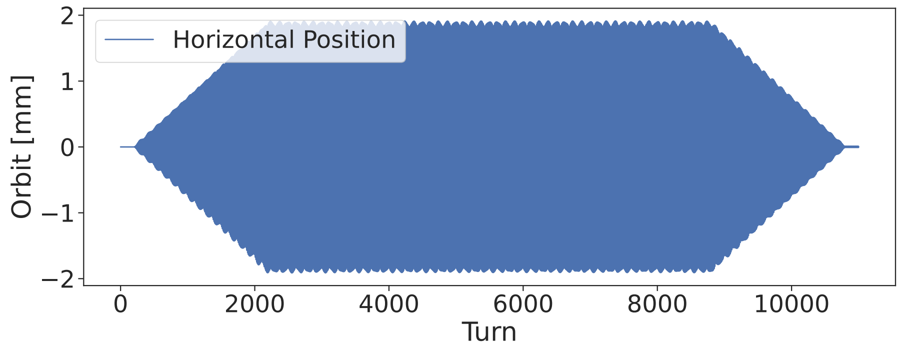

Figure 3.2.: Simulated turn by turn data with an AC-Dipole first ramping up then down.

3.2. Correction Principles

3.2.1. Response Matrix

A response matrix is a linear equation system that describes the change of an observable for a set of individual multipole strengths. By taking the pseudo-inverse of this matrix and multiplying it to the measured observables, a set of corrector strengths if obtained that can replicate the measured value. Taking the opposite sign then gives a correction. This technique is routinely used to correct, amongst others, β-beating as well as Resonance Driving Terms. In situations where measurements are taken at each BPM for a particular observable, the corresponding response matrix ends up containing over 500 values per corrector, for a single beam.

Individual MAD-X simulations are run with a single multipole powered at a time. The resulting parameter values (e.g. β-beating) are then compared to those obtained from a simulation without any powering, allowing to determine the specific impact of each multipole.

A response matrix is thus created following Eq. (3.2), for a matrix of observables O, a reference matrix of observables without any corrector O_R and a fixed multipole strength k. Given measured data M, the set of correctors needed to compensate the values can be obtained by taking the pseudo-inverse of the matrix in Eq. (3.3).

$$R = (O - O_R) \cdot \frac{1}{k} \tag{3.2}$$

$$\begin{bmatrix} k_1 \\ \vdots \\ k_n \end{bmatrix} = -(R^+ \cdot M) \tag{3.3}$$

Response matrices are very versatile and can combine several observables to be corrected by the same multipoles. One example, detailed later in this thesis, is the third order chromaticity and the resonance driving term f_{1004}, both contributed to by decapoles.

Example

In this example, simulations are run with MAD-X PTC to correct the third chromaticity in the LHC. Q''' is taken from `ptc_normal` for each beam and axis, with MCDs, decapole correctors, powered with a fixed strength one at a time. A scaling factor is applied to get the change of chromaticity for one unit of K_5. 8 correctors are used, which strengths are denoted k_1 through k_8. Transposes are only used to make the equations easier to display.
The values in Tab.3.1 are corrected via Eq. (3.5) after having built the response matrix in Eq. (3.4).

Observable	Value
Q_x'''	-666111
Q_y'''	121557

Table 3.1.: Example chromaticity values to correct via a response matrix

$$R = \left(\text{Individual simulations} \left\{ \overbrace{\begin{bmatrix} -155899 & 122004 \\ -254584 & 138368 \\ -122715 & 106709 \\ -218597 & 110686 \\ -134140 & 106463 \\ -245791 & 118951 \\ -147035 & 116544 \\ -219537 & 112317 \end{bmatrix}}^{Q_x''' \quad\quad Q_y'''}{}^{T} - \overbrace{\begin{bmatrix} 5135 \\ 8470 \end{bmatrix}}^{\text{Reference}} \right\} \begin{matrix} Q_x''' \\ Q_y''' \end{matrix} \right) \cdot \underbrace{\frac{1}{-1000}}_{\text{Corrector strength}} \tag{3.4}$$

$$\begin{matrix} k_1 \\ k_2 \\ k_3 \\ k_4 \\ k_5 \\ k_6 \\ k_7 \\ k_8 \end{matrix} \left\{ \begin{pmatrix} -1235 \\ 1032 \\ -1394 \\ 1449 \\ -1043 \\ 1864 \\ -1187 \\ 1369 \end{pmatrix} \right. = -R^{+} \cdot \left. \begin{pmatrix} -666111 \\ 121557 \end{pmatrix} \right\} \begin{matrix} \text{Measured} \\ \text{values} \end{matrix} \tag{3.5}$$

3.2.2. Chromaticity

As per the placement of the MCO and MCD spool piece correctors in the LHC layout [22], β-functions at their location are slightly different from arc to arc. This slight imbalance leads theoretically to the possibility of correcting the horizontal and vertical axes of the second and third order chromaticity independently, via a response matrix approach. In practice, the required strength to do so would exceed those of the design of the correctors.

Another way to correct the chromaticity is via a global uniform trim, where every available corrector is powered to the same strength. Simulations are run with `ptc_normal` via MADX-PTC to obtain the response in chromaticity for a given strength. Chromaticity being linear with multipole strength, an affine function can be determined for each axis. Figure 3.3 shows a simulation with several MCD strengths, highlighting this linear relation between Q''' and K_5, while Equation (3.6) shows an example of such functions computed at injection energy for the 2022 optics.

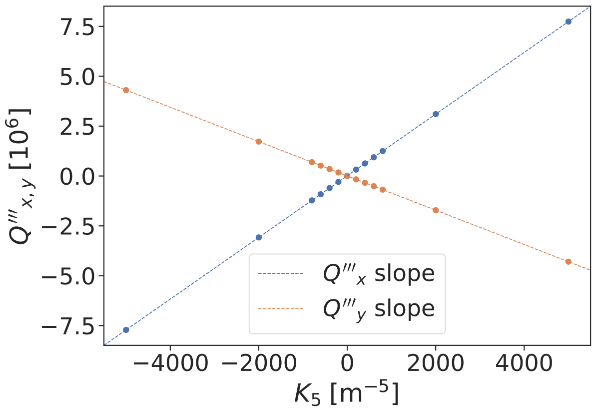

Figure 3.3.: Linear relation between the third order chromaticity and decapole corrector strengths, simulated with MADX-PTC.

$$\begin{aligned} Q_x''' &= 1533 \cdot \Delta K_5 + 6680 \\ Q_y''' &= -860 \cdot \Delta K_5 + 5647 \end{aligned} \tag{3.6}$$

Only the linear part is relevant, as the offset is generated by other multipoles and field errors. It is thus constant for a configuration where only the relevant spool pieces are used.

Corrections involve minimizing both axes, typically where Q_x''' meets Q_y''':

$$\Delta K_5 = -\frac{(Q_x''' - Q_y''')}{\text{slope}_{Q_x'''} - \text{slope}_{Q_y'''}} \tag{3.7}$$

3.3. Optics Measurements

3.3.1. Linear Optics

Excitation via ac dipole
spectral analysis
optics reconstruction

3

3.3.2. Chromaticity

Procedure

Chromaticity measurements are typically performed by varying the RF frequency to induce a change of momentum offset δ, while measuring the tune. The momentum offset δ being related to the RF frequency and the momentum compaction factor α_c:

$$\delta = -\frac{1}{\alpha_c} \cdot \frac{\Delta f_{\mathrm{RF}}}{f_{\mathrm{RF,nominal}}} \tag{3.8}$$

Frequency steps of 20Hz every 30 secondes are usually taken to compromise between number of data points, precision of the tune estimate, and duration of the measurement. Once beam losses, registered by the BLMs are deemed too high, the frequency is reverted back to its nominal value in larger steps. The same procedure is then re-applied in the negative. Figure 3.4 shows a typical RF scan performed to measure chromaticity in the LHC.

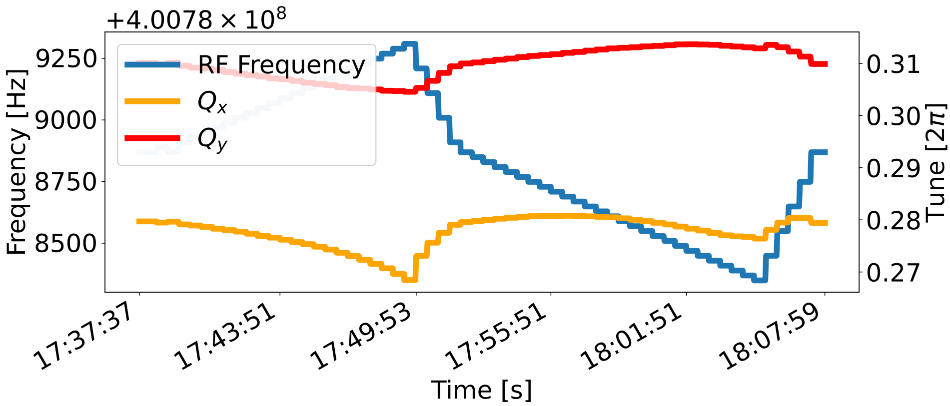

Figure 3.4.: Observation of the tune dependence on momentum offset, created by a shift of RF frequency.

Analysis

Once the tunes have been acquired and the momentum offset computed via Eq. (3.8), the chromaticity function (see Eq.(2.57)) can be used to fit the measured data and retrieve each order.

As part of work for this thesis, a custom tool was developed, in order to ease such analysis of chromaticity measurements. This tool, the Non-Linear Chromaticity GUI [23], is composed of several parts:

- Data extraction from CERN data servers (Timber, NXCALS)
- Tune cleaning and standard deviation calculation
- Chromaticity fit up to 7th order
- Corrections of chromaticity and resonance driving terms

if the screenshot actually useful?

Fits up to the third and fifth order using this tool can be seen in Fig.3.5.

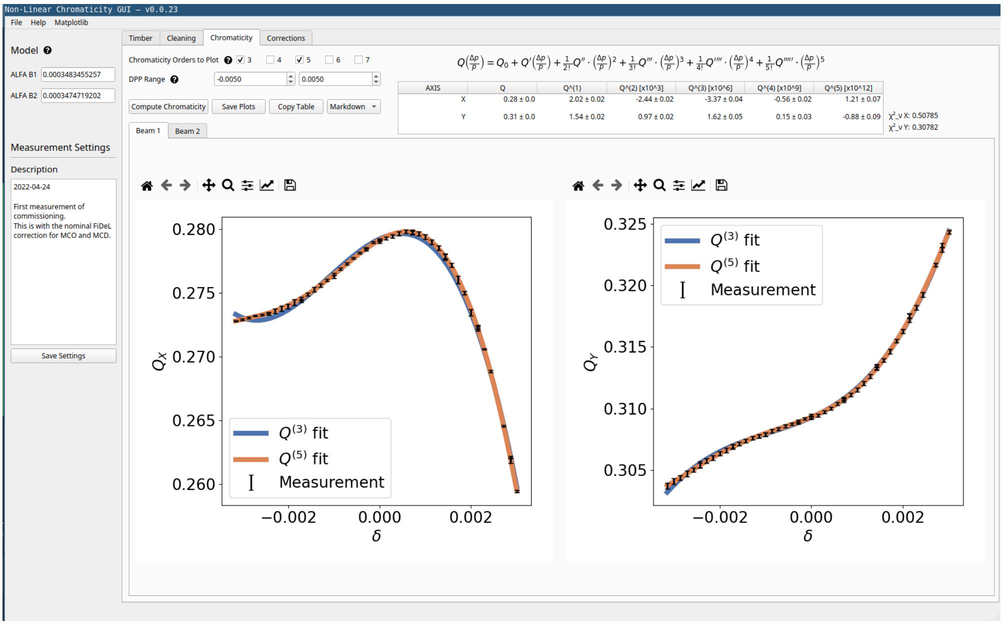

Figure 3.5.: *Non-Linear Chromaticity GUI* program, used to automatize chromaticity analysis.

4

The Art of Measuring and Correcting Decapole Effects in the Large Hadron Collider

Contents

4.1. Motivation

The decapole fields in the LHC have been studied since Run 1 via chromaticity measurements [24–26]. The third order of the non-linear chromaticity, Q''', generated for the most part by decapoles, has shown a consistent discrepancy at injection energy between its expected value in simulation and that observed in beam-based measurements. Figure 4.1 highlights this discrepancy.

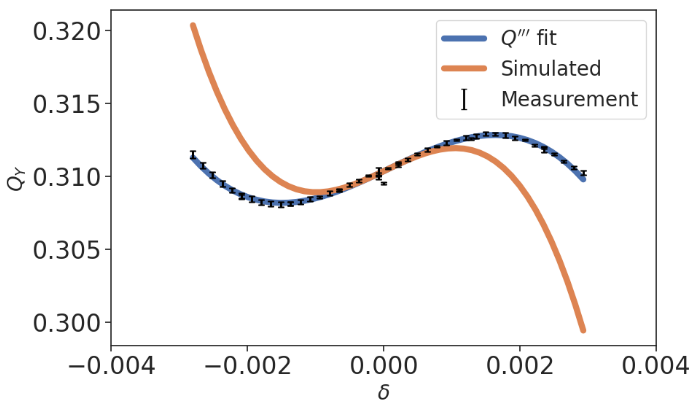

Figure 4.1.: Measured and simulated chromaticity at injection energy without octupolar and decapolar corrections. **png really?**

This discrepancy poses a significant problem, as the operational corrections are derived from simulations. It is thus observed that Q''' is over-corrected by an almost factor 2, resulting in an effectively un-corrected third order chromaticity. Chromaticity measurements have thus been repeated during LHC's Run 3 and complemented by beam-based corrections.

While non-linear chromaticity provides an easy measurement of decapolar fields, it does not permit alone to understand where the discrepancy originates from. New measurements were therefore undertaken to better understand the decapolar fields via observables never studied before:

- Bare Chromaticity, chromaticity with octupolar and decapolar correctors turned off.
- Chromatic Amplitude Detuning, tune shift dependant on both the action and the momentum offset.
- Resonance Driving Term f_{1004}, contributing to a resonance close the working point.

4.2. Non-Linear Chromaticity

4.2.1. Introduction

Expression Chromaticity is the tune shift $\Delta Q_{x,y}$ dependent on the momentum offset δ of a particle. Its general expression is given by a Taylor expansion in Eq. (2.57). The full third term is highlighted in the following,

$$Q(\delta) = Q_0 + Q'\delta + \frac{1}{2!}Q''\delta^2 + \boxed{\frac{1}{3!}Q'''\delta^3} + \mathcal{O}(\delta^4). \tag{4.1}$$

It is to be noted when referring to a chromaticity order, that the preceding fraction and δ are usually *not* included in the term. This third order is mainly contributed to by decapoles. It is related to the β-function, the dispersion and the strength of the multipole, also shown in Eq. (2.69):

$$\begin{aligned} \Delta Q_x''' &= \frac{1}{4\pi}K_5 L\beta_x D_x^3 \\ \Delta Q_y''' &= -\frac{1}{4\pi}K_5 L\beta_x D_x^3. \end{aligned} \tag{4.2}$$

Correction Q''' is linear with the decapole strength. As such, it can be easily corrected via global trims presented in Section 3.2.2. A change of decapole strength $K_5 = 1000$ would for example have the following impact with the injection optics used in 2022:

$$\Delta Q_x = 1.5 \times 10^6 \quad ; \quad \Delta Q_x = -0.9 \times 10^6. \tag{4.3}$$

4.2.2. Measurement

Chromaticity is measured by varying the frequency of the radio-frequency (RF) cavities, used to create buckets and to accelerate the beam. The change in δ related to this frequency is, as a reminder:

$$\delta = -\frac{1}{\alpha_c} \cdot \frac{\Delta f_{RF}}{f_{RF,nominal}}. \tag{4.4}$$

More details on the measurements and analysis can be found in earlier Section 3.3.2.

Momentum Compaction Factor Rather than a constant, the momentum compaction factor is an expansion, as detailed in **ref to α_c in concepts of accelerators**. It is assumed here though to be constant.

4.2.3. blabla

Measurements were taken during 2022 Commissioning for

- Beam Test
- Commissioning
  - FiDeL
  - Q"' corr
  - Q" corr
- 60° optics

Also during MD6864, 2022-10-19, for the bare machine
Also 2022-11-06, measurement at 30cm, flat top.

High order α_c.
Radial loop instead of formula.

4.3. Chromatic Amplitude Detuning

4.4. Resonance Driving Terms

Measurements

- 2022 Q” and Q”’ corrections 2022-04-24
- 2022-10-19 Virgin machine
- 2023-easter (FiDeL)
- 2023-06-14 MD9549 (FiDeL and Q”’/ RDT corr)

Bring up effect of KCO on RDT f1004

4.4.1. Decapolar Contribution

4.4.2. Lower Order Contributions

4.5. Impact of Decapolar Fields

4.6. Integrating Decay

5

Very High Order Field Measurement in the LHC

Contents

5.1. First Measurement of Fourth and Fifth Order Chromaticity

1. comparison to Ewen's measurements done with dpp from timber
2. IPAC paper basically
3. b6 meas from 2024 commissioning
4. higher order momentum compaction factor => twiss at different dpp fit vs ptc

5.2. INTRODUCTION

5

Non-Linear chromaticity measurements at injection have been performed since Run 1 [**maclean:ipac11-wepc078**, **maclean:ipac16-thpmr039**, 25, 27]. Those measurements, made by varying the RF frequency while observing the resulting tune change, have been carried out with a momentum offset of up to $\delta = \pm 2.2 \times 10^{-3}$, which led to the observation of the third order term of the non-linear chromaticity.

During the commissioning of Run 3, a new collimator sequence was introduced, allowing wider momentum offset measurements, within $\delta \in [-3.2 \times 10^{-3}, 3.7 \times 10^{-3}]$. This improved setup led to the observation of the fourth and fifth order terms at injection energy, denoted $Q^{(4)}$ and $Q^{(5)}$ respectively, produced to first order by dodecapoles and decatetrapole (see section NL-CHROMATICITY MODEL):

$$\begin{aligned} Q(\delta) = Q_0 + Q'\delta + \frac{1}{2!}Q''\delta^2 + \frac{1}{3!}Q'''\delta^3 \\ + \frac{1}{4!}Q^{(4)}\delta^4 + \frac{1}{5!}Q^{(5)}\delta^5 + O(\delta^6). \end{aligned} \tag{5.1}$$

The momentum offset δ is related to the RF frequency and the momentum compaction factor:

$$\delta = -\frac{1}{\alpha_c}\frac{\Delta f_{RF}}{f_{RF,nominal}}.$$

The model α_c used is 3.48×10^{-4} for beam 1 and 3.47×10^{-4} for beam 2. Via this relation, a change of 140Hz of the RF frequency corresponds to a momentum offset of about -0.001.

Results of $Q^{(4)}$ and $Q^{(5)}$ measurements are presented, along with a comparison to the model.

5.3. NL-CHROMATICITY MEASUREMENTS

Two chromaticity measurements were performed with different settings. The first one used the nominal correction strengths for octupole and decapole corrector magnets, derived from magnetic measurements, where the second one used beam-based corrections for the same elements, computed from measurements. Those two measurements have a respective momentum-offset range of $[-3.1 \times 10^{-3}, 3.1 \times 10^{-3}]$ and $[-3.2 \times 10^{-3}, 3.7 \times 10^{-3}]$.

5.3.1. Nominal Corrections

A first chromaticity measurement was performed during the LHC beam commissioning in April 2022. The horizontal and vertical tunes were set to 0.28 and 0.31. Q' was reduced to a value of 2 to allow for a better identification of the higher order terms. The standard measurement procedure was then applied, by varying the RF frequency to induce a change in momentum offset. Frequency steps of 20Hz were taken roughly every 30 seconds, to allow for a precise tune measurement. Once beam losses, registered by the beam loss monitors (BLM), are deemed too high the frequency is reverted back to its nominal frequency in larger steps. Figure 5.1 shows a typical RF scan performed to measure chromaticity.

At very high momentum-offsets, the Base-Band Tune system (BBQ) [28, 29] was found not to give reliable tune measurements. A new approach using custom post-processing of the raw BBQ turn-by-turn data was therefore developed, giving more precise tune measurements by performing spectral analysis with an increased number

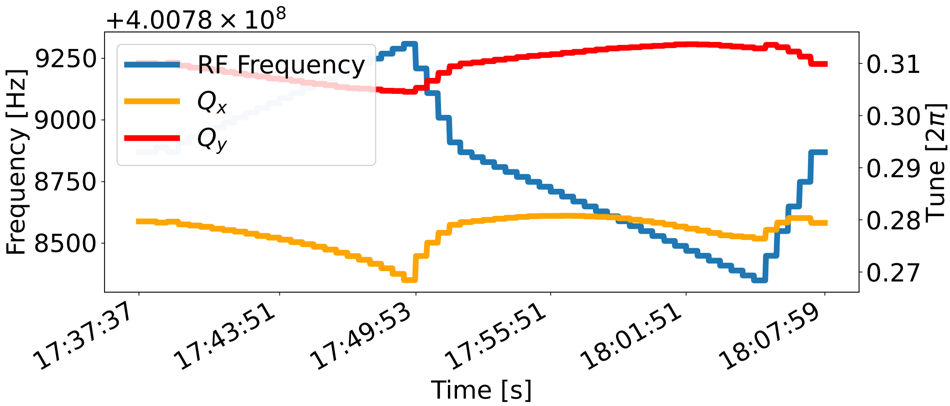

Figure 5.1.: Observation of the tune dependence on momentum offset, created by a shift of RF frequency.

5

of turns to improve the signal to noise ratio. Further cleaning is then applied by removing outliers and identified noise lines.

The octupole and decapole correctors were set to their nominal settings. Results of this initial measurement are shown in Tab. 5.1. Lower order chromaticities such as Q' and Q'' are consistent with previous measurements [25].

	$Q^{(2)}\,[10^3]$	$Q^{(3)}\,[10^6]$	$Q^{(4)}\,[10^9]$	$Q^{(5)}\,[10^{12}]$
B1				
X	-2.44 ± 0.02	-3.36 ± 0.04	-0.56 ± 0.02	1.20 ± 0.07
Y	0.97 ± 0.02	1.62 ± 0.05	0.15 ± 0.03	-0.88 ± 0.09
B2				
X	-2.45 ± 0.03	-2.72 ± 0.08	-1.00 ± 0.05	0.15 ± 0.14
Y	0.79 ± 0.03	1.54 ± 0.06	0.24 ± 0.04	-0.74 ± 0.13

Table 5.1.: Terms of the high order chromaticity obtained during Run 3 commissioning in April 2022, with nominal corrections.

Due to the momentum offset being zero several times during the measurement, it was possible to determine that the tune drift is negligible. The measurement was also performed after an extended period at injection energy, where the b_3 decay is small and not causing any change in the first order chromaticity. The fitted curve for the chromaticity function is shown in Fig. 5.2. It can be seen that a higher order polynomial is beneficial for the fit, as discussed further in "$Q^{(4)}$ and $Q^{(5)}$ fit quality".

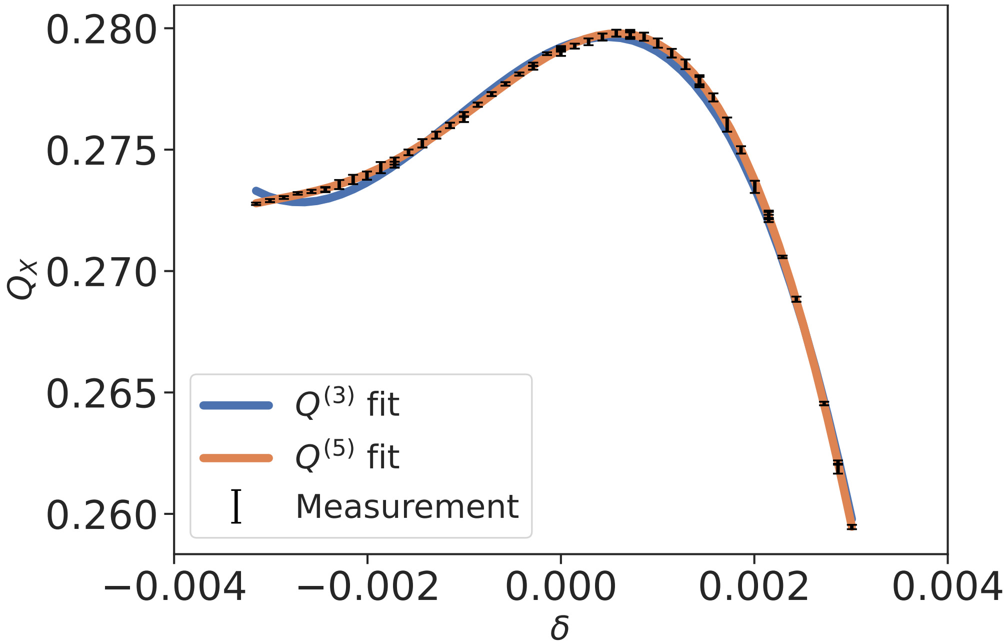

Figure 5.2.: Beam 1 measurement of higher order chromaticity terms with nominal corrections used during operation. Fits are up to the third and fifth order.

5.3.2. Beam-Based Corrections

After correcting the second and third order chromaticities via the octupole and decapole correctors, a second measurement was performed. A uniform trim on all the correctors of each class was applied for each beam, resulting in a global correction. A total of four circuits were unavailable for the octupoles, three for beam 1 and one for

5

beam 2, resulting in larger corrections for beam 1. Corrections applied on top of the nominal settings [25] for the octupoles and decapoles are shown in Tab. 5.2.

Beam	$K_4\,[\mathrm{m}^{-4}]$	$K_5\,[\mathrm{m}^{-5}]$
1	+3.2973	+1610
2	+2.1716	+1618

Table 5.2.: Corrections applied on top of the nominal octupole and decapole correctors strengths.

Figure 5.3 shows the chromaticity fit after the beam-based minimization of Q'' and Q''', while Table 5.3 shows the measured chromaticity.

Previous studies of chromaticity in the LHC only considered fits up to third-order. Including fits up to a fifth order increases the Q''' estimate of both measurements, while improving the fit quality. Q''' for beam 1 with only a fit to the third order would have a value of -0.38×10^6 instead of the -1.02×10^6 obtained with a fifth order fit. Accurately measuring the third order chromaticity is essential in order to correct it.

	$Q^{(2)}\,[10^3]$	$Q^{(3)}\,[10^6]$	$Q^{(4)}\,[10^9]$	$Q^{(5)}\,[10^{12}]$
B1				
X	-0.62 ± 0.01	-1.02 ± 0.03	-0.63 ± 0.02	1.22 ± 0.05
Y	-0.24 ± 0.01	0.12 ± 0.02	0.04 ± 0.02	-0.56 ± 0.04
B2				
X	-0.85 ± 0.01	-0.64 ± 0.03	-0.58 ± 0.02	1.07 ± 0.06
Y	-0.30 ± 0.02	0.14 ± 0.03	0.16 ± 0.02	-0.66 ± 0.05

Table 5.3.: Terms of higher order chromaticity obtained during Run 3 commissioning in April 2022, with beam-based corrections for Q'' and Q'''.

5.3.3. $Q^{(4)}$ and $Q^{(5)}$ fit quality

The values measured for $Q^{(4)}$ and $Q^{(5)}$ are similar across the two measurements, with nominal and beam-based corrections performed with very different lower order chromaticity and several hours apart. This reproducibility gives confidence that

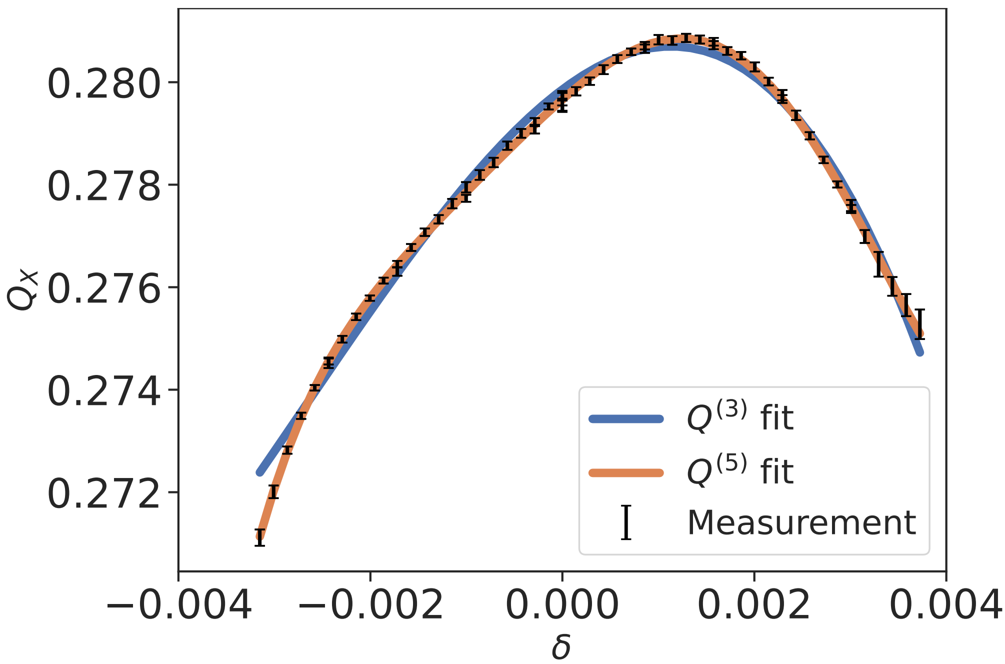

Figure 5.3.: Beam 1 measurement of high order chromaticity terms after application of Q'' and Q''' beam-based corrections on octupole and decapole correctors.

the measured values are robust. It is to be noted that one exception exists, for the horizontal plane of beam 2, where the measurement with nominal correction settings showed a high correlation between the fourth and fifth order terms, making the fit less reliable.

The reduced chi-square for the last measurement for each fit order is detailed in Tab. 5.4, where it can be seen that a fit above fifth order does not improve the fit quality.

Plane	$\chi^2_\nu\ Q^{(3)}$	$\chi^2_\nu\ Q^{(4)}$	$\chi^2_\nu\ Q^{(5)}$	$\chi^2_\nu\ Q^{(6)}$
Beam 1				
X	17.9	12.1	1.8	1.47
Y	3.0	2.2	0.7	0.7
Beam 2				
X	17.3	7.1	1.8	1.76
Y	2.9	2.8	1.0	1.0

Table 5.4.: Reduced χ^2_ν values for each order of fit, taken from the last commissioning measurement.

5.4. NL-CHROMATICITY MODEL

The model of the LHC is based on MADX and WISE field errors [30]. To compute the chromaticity, simulations are run via the Polymorphic Tracking Code (PTC), with field errors from sextupole to decahexapole loaded and applied on all magnets. Simulation results are shown in Tab. 5.5.

Table 5.6 shows the ratio between measured and simulated high-order chromaticity. The measured $Q^{(5)}$ shows a consistent discrepancy with the model, larger by about a factor 2.

Plane	$Q^{(4)}\,[10^9]$	$Q^{(5)}\,[10^{12}]$
Beam 1		
X	-0.2 ± 0.1	0.7 ± 0.1
Y	0.1 ± 0.1	-0.3 ± 0.1
Beam 2		
X	-0.2 ± 0.1	0.8 ± 0.1
Y	0.1 ± 0.1	-0.4 ± 0.1

Table 5.5.: Simulated high order chromaticity terms via PTC, including field errors from b_3 to b_8 with the previous beam-based corrections.

Simulations with only b_6 and b_7 field errors have been run to assess the contribution of lower order magnets to the fifth order chromaticities. The results strongly imply

Plane / Measurement	$Q^{(5)}$ ratio first	$Q^{(5)}$ ratio second
Beam 1		
X	1.8 ± 0.1	1.8 ± 0.1
Y	2.7 ± 0.3	1.7 ± 0.1
Beam 2		
X		1.6 ± 0.1
Y	2.2 ± 0.4	1.9 ± 0.2

Table 5.6.: Ratios of the measured to simulated fifth order chromaticity term for both first and second measurements. The values are taken from tables 5.1, 5.3 and 5.5. The fit with high correlation was not included.

that the decatetrapole errors are the main contributors to $Q^{(5)}$, as can be seen in Fig. 5.4. Fringe fields and skew multipoles have been found to have a negligible impact. Ongoing studies are assessing the contribution of β-beating, linear coupling and alignment errors to those estimates.

5

5.5. CONCLUSIONS AND OUTLOOK

A wider momentum offset range, combined with new analysis techniques permitted the observation of fourth and fifth order chromaticity for the first time in the LHC. Reproducible values were measured with different machine configurations. Preliminary simulations show that the observed values do not match well with the LHC non-linear model. A factor 2 is observed between beams and planes for $Q^{(5)}$, which may point to a systematic error in the b7 error model.

Correction of the measured higher order chromaticity terms is not possible, due to the lack of adequate correctors in the LHC. It is nevertheless interesting to characterize the higher order errors for an effective model and understand the effect a higher order fit has on lower order terms. Precise measurement of those lower chromaticity terms is required in order to effectively correct them. Higher order terms have thus to be taken into account.

The current range of momentum offset is deemed sufficient to measure higher order chromaticity. Attempts will, however, be taken to increase that range and assess if such a wider range can refine the estimate of $Q^{(4)}$ and $Q^{(5)}$.

5.6. First Measurement of Dodecapole RDTs

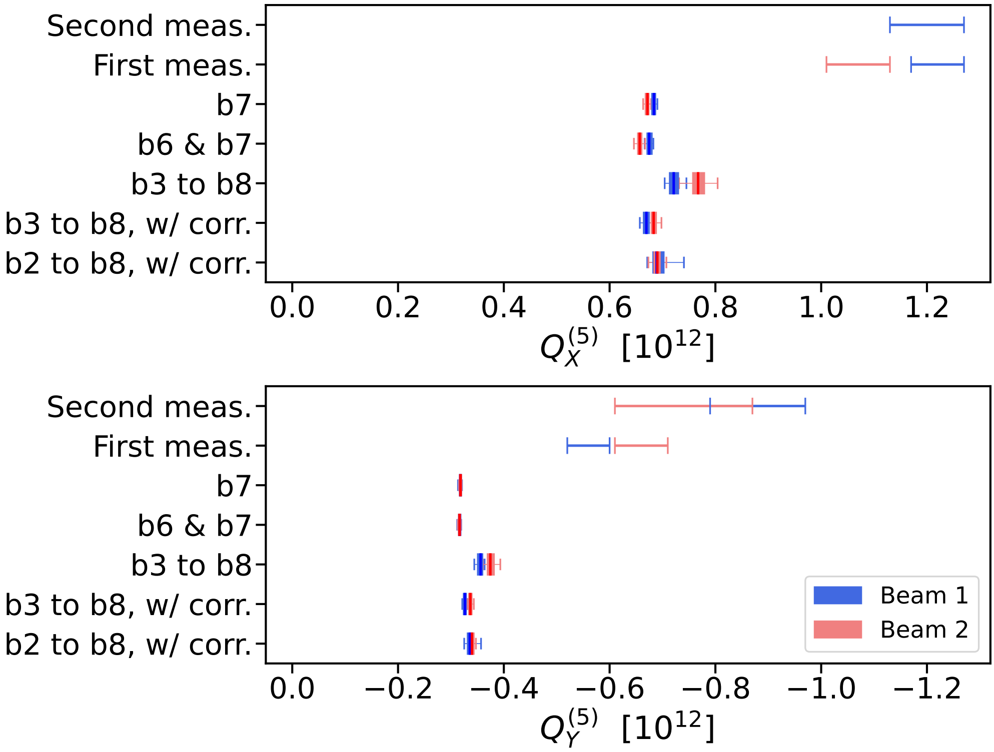

Figure 5.4.: Measured and simulated fifth order chromaticity. The simulations are done via PTC and include different multipole errors, some of them further include the nominal corrections for b_3, b_4 and b_5. The b_2 errors, applied on dipoles and quadrupoles, generate beta-beating. The measurement with a high correlation is not included.

6

Skew Octupole Fields in the LHC

Contents

6.1. Correction of skew octupole Fields at Top Energy

1. RDT Measurements
2. Orthogonality of correctors
3. Response Matrix
4. Correction
5. Comparison to 2018

6.2. Correction of Skew Octupole Fields at Injection Energy

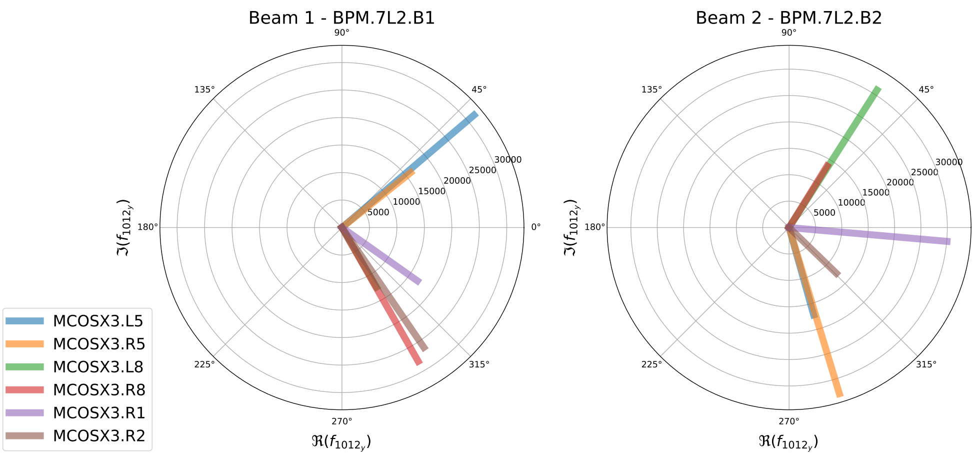

Figure 6.1.

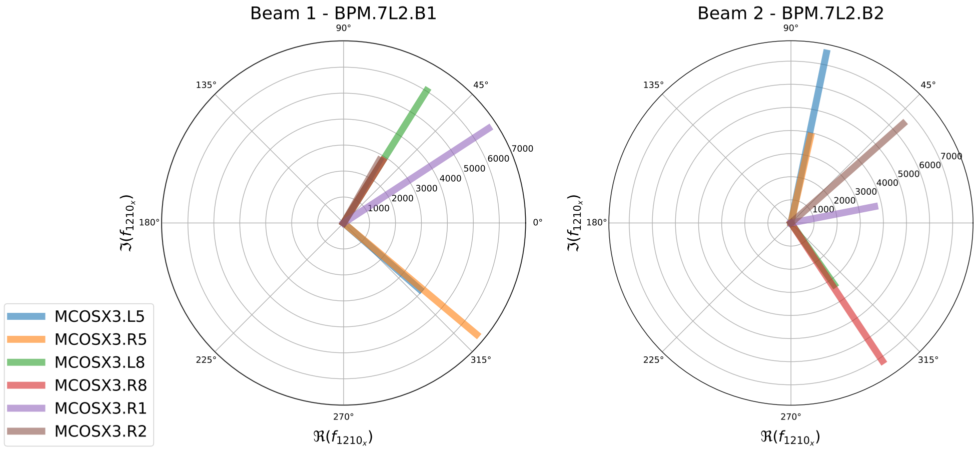

Figure 6.2.

6.3. Skew Octupolar Fields from Landau Octupoles

A

Units and Conversions

A.1. Physical Constants

Name	Symbol	Value	Unit
Speed of light in vacuum	c	2.99792458×10^8	m/s
Elementary charge	e	1.60217663×10^9	C

Table A.1.: Physical Constants

A.2. Units

A.3. Conversions

A

A

B

Hamiltonians and Transfer Maps

This appendix is intended to gather and explicit the Hamiltonians of the elements used in this thesis. Non-linear transfer maps are also described for some of those elements from the first to the second order.

B.1. Hamiltonians of Elements

The Hamiltonian of a *multipole* is the following [4–6]:

$$H = \Re\left[\sum_{n>1}(K_n + iJ_n)\frac{(x+iy)^n}{n!}\right]. \tag{B.1}$$

From this, normal and skew fields can be separated:

$$\begin{aligned} N_n &= \frac{1}{n!}K_n\Re\left[(x+iy)^n\right] \\ S_n &= -\frac{1}{n!}J_n\Im\left[(x+iy)^n\right], \end{aligned} \tag{B.2}$$

where K and J are the normalized strength of the multipole and x, y the transverse coordinates. Table B.1 explicits the normal and skew Hamiltonians of multipoles up to order 8.

Name	Order	Normal and Skew Hamiltonians
Drift	-	$H = \frac{1}{2}(p_x^2 + p_y^2)$
Quadrupole	2	$N_2 = \frac{1}{2!}K_2\left(x^2 - y^2\right)$ $S_2 = -J_2 xy$
Sextupole	3	$N_3 = \frac{1}{3!}K_3\left(x^3 - 3xy^2\right)$ $S_3 = -\frac{1}{3!}J_3 \cdot \left(3x^2y - y^3\right)$
Octupole	4	$N_4 = \frac{1}{4!}K_4\left(x^4 - 6x^2y^2 + y^4\right)$ $S_4 = -\frac{1}{4!}J_4 \cdot \left(4x^3y - 4xy^3\right)$
Decapole	5	$N_5 = \frac{1}{5!}K_5\left(x^5 - 10x^3y^2 + 5xy^4\right)$ $S_5 = -\frac{1}{5!}J_5 \cdot \left(5x^4y - 10x^2y^3 + y^5\right)$
Dodecapole	6	$N_6 = \frac{1}{6!}K_6\left(x^6 - 15x^4y^2 + 15x^2y^4 - y^6\right)$ $S_6 = -\frac{1}{6!}J_6 \cdot \left(6x^5y - 20x^3y^3 + 6xy^5\right)$
Decatetrapole	7	$N_7 = \frac{1}{7!}K_7\left(x^7 - 21x^5y^2 + 35x^3y^4 - 7xy^6\right)$ $S_7 = -\frac{1}{7!}J_7 \cdot \left(7x^6y - 35x^4y^3 + 21x^2y^5 - y^7\right)$
Decahexapole	8	$N_8 = \frac{1}{8!}K_8\left(x^8 - 28x^6y^2 + 70x^4y^4 - 28x^2y^6 + y^8\right)$ $S_8 = -\frac{1}{8!}J_8 \cdot \left(8x^7y - 56x^5y^3 + 56x^3y^5 - 8xy^7\right)$

Table B.1.: Normal and skew Hamiltonians of multipoles up to order 8.

B.2. Transfer Maps

This sections goes more in depth regarding the derivation of the examples of transfer maps introduced in Section 2.4.

As a reminder, the BCH of two elements up to order 3 is given below,

$$Z = \underbrace{H_2 + H_1}_{\text{First order}} + \underbrace{\frac{[H_2, H_1]}{2}}_{\text{Second order}} + \underbrace{\frac{[H_2, [H_2, H_1]]}{12} - \frac{[H_1, [H_2, H_1]]}{12}}_{\text{Third order}}. \tag{B.3}$$

B

B.2.1. Generic Effective Hamiltonian of Two Elements

Two elements of orders n and m can be combined together via the BCH. Below are detailed the multipole-like orders that are generated depending on the BCH order.

First Order

$$\text{multipolar-like orders} = \begin{cases} m \\ n \end{cases} . \tag{B.4}$$

Second Order

$$\text{multipolar-like orders} = \begin{cases} m + n - 2 \end{cases} . \tag{B.5}$$

Third Order

$$\text{multipolar-like orders} = \begin{cases} m + 2n - 4 \\ 2m + n - 4 \end{cases} . \tag{B.6}$$

B.2.2. Transfer Map of Two Sextupoles

The transfer map of two sextupoles H_1 and H_2 of strength K_1 and K_2, separated by a drift to introduce a change of coordinates in H_1 is the following,

$$\mathcal{M} = e^{:Z:} = e^{:H_2:} \cdot e^{D:H_1:}, \tag{B.7}$$

After such application of the drift on H_1, the two hamiltonians read,

$$\begin{aligned} H_1 &= \frac{1}{3!} K_{3,h1} L_1 \left((L_D p_x + x)^3 - 3 (L_D p_x + x) \left(L_D p_y + y \right)^2 \right) \\ H_2 &= \frac{1}{3!} K_2 L_2 \left(x^3 - 3xy^2 \right) . \end{aligned} \tag{B.8}$$

Below are detailed each term of the BCH. Each term should be added together in order to obtain the whole effective Hamiltonian Z.

First Order

$$\left.\begin{aligned}
&K_1 L_1 L_D \left(\begin{aligned} &\frac{L_D^2 p_x^3}{6} - \frac{L_D^2 p_x p_y^2}{2} + \frac{L_D p_x^2 x}{2} - L_D p_x p_y y \\ &- \frac{L_D p_y^2 x}{2} + \frac{p_x x^2}{2} - \frac{p_x y^2}{2} - p_y x y \end{aligned} \right) \\
&+ K_1 L_1 \left(\frac{x^3}{6} - \frac{x y^2}{2} \right) + K_2 L_2 \left(\frac{x^3}{6} - \frac{x y^2}{2} \right)
\end{aligned} \right\} \text{sextupolar} \tag{B.9}$$

Second Order

$$K_1 K_2 L_1 L_2 L_D \left(\left(\begin{aligned} &\frac{L_D^2 p_x^2 x^2}{8} - \frac{L_D^2 p_x^2 y^2}{8} + \frac{L_D^2 p_x p_y x y}{2} - \frac{L_D^2 p_y^2 x^2}{8} \\ &+ \frac{L_D^2 p_y^2 y^2}{8} + \frac{L_D p_x x^3}{4} + \frac{L_D p_x x y^2}{4} + \frac{L_D p_y x^2 y}{4} \\ &+ \frac{L_D p_y y^3}{4} + \frac{x^4}{8} + \frac{x^2 y^2}{4} + \frac{y^4}{8} \end{aligned} \right) \right\} \text{octupolar-like} \tag{B.10}$$

Third Order

$$\left.\begin{aligned}
&K_1^2 K_2 L_1^2 L_2 L_D \left(\begin{aligned} &\frac{L_D^5 p_x^4 x}{48} + \frac{L_D^5 p_x^3 p_y y}{12} - \frac{L_D^5 p_x^2 p_y^2 x}{8} - \frac{L_D^5 p_x p_y^3 y}{12} \\ &+ \frac{L_D^5 p_y^4 x}{48} + \frac{L_D^4 p_x^3 x^2}{12} + \frac{L_D^4 p_x^3 y^2}{12} - \frac{L_D^4 p_x p_y^2 x^2}{4} \\ &- \frac{L_D^4 p_x p_y^2 y^2}{4} + \frac{L_D^3 p_x^2 x^3}{8} + \frac{L_D^3 p_x^2 x y^2}{8} - \frac{L_D^3 p_x p_y x^2 y}{4} \\ &- \frac{L_D^3 p_x p_y y^3}{4} - \frac{L_D^3 p_y^2 x^3}{8} - \frac{L_D^3 p_y^2 x y^2}{8} + \frac{L_D^2 p_x x^4}{12} \\ &- \frac{L_D^2 p_x y^4}{12} - \frac{L_D^2 p_y x^3 y}{6} - \frac{L_D^2 p_y x y^3}{6} + \frac{L_D x^5}{48} \\ &- \frac{L_D x^3 y^2}{24} - \frac{L_D x y^4}{16} \end{aligned} \right) \\
&+ K_1 K_2^2 L_1 L_2^2 L_D \left(\begin{aligned} &\frac{L_D^2 p_x x^4}{48} - \frac{L_D^2 p_x x^2 y^2}{8} + \frac{L_D^2 p_x y^4}{48} + \frac{L_D^2 p_y x^3 y}{12} \\ &- \frac{L_D^2 p_y x y^3}{12} + \frac{L_D x^5}{48} - \frac{L_D x^3 y^2}{24} - \frac{L_D x y^4}{16} \end{aligned} \right)
\end{aligned} \right\} \text{decapolar-like} \tag{B.11}$$

B

B.2.3. Transfer Map of a Sextupole and Octupole

The transfer map of a sextupole H_1 and octupole H_2 of strength K_1 and K_2, separated by a drift like in the previous example is given by

$$\mathcal{M} = e^{:Z:} = e^{:H_2:} \cdot e^{D:H_1:} \tag{B.12}$$

with H_1 and H_2 having as final expressions,

$$\begin{aligned} H_1 &= \frac{1}{3!} K_{3,h1} L_1 \left((L_D p_x + x)^3 - 3 \left(L_D p_x + x\right) \left(L_D p_y + y\right)^2 \right) \\ H_2 &= \frac{1}{4!} K_2 L_2 \left(x^4 - 6x^2 y^2 + y^4 \right). \end{aligned} \tag{B.13}$$

The first two orders of the BCH of those two elements is given below.

First Order

$$\begin{aligned} &\left. K_3 \begin{pmatrix} \frac{L_D^3 p_x^3}{6} - \frac{L_D^3 p_x p_y^2}{2} + \frac{L_D^2 p_x^2 x}{2} - L_D^2 p_x p_y y - \frac{L_D^2 p_y^2 x}{2} \\ + \frac{L_D p_x x^2}{2} - \frac{L_D p_x y^2}{2} - L_D p_y x y + \frac{x^3}{6} - \frac{x y^2}{2} \end{pmatrix} \right\} \text{sextupolar} \\ &\left. + K_4 \left(\frac{x^4}{24} - \frac{x^2 y^2}{4} + \frac{y^4}{24} \right) \right\} \text{octupolar} \end{aligned} \tag{B.14}$$

Second Order

$$\left. K_3 K_4 L_D \begin{pmatrix} \frac{L_D^2 p_x^2 x^3}{24} - \frac{L_D^2 p_x^2 x y^2}{8} + \frac{L_D^2 p_x p_y x^2 y}{4} - \frac{L_D^2 p_x p_y y^3}{12} \\ - \frac{L_D^2 p_y^2 x^3}{24} + \frac{L_D^2 p_y^2 x y^2}{8} + \frac{L_D p_x x^4}{12} - \frac{L_D p_x y^4}{12} \\ + \frac{L_D p_y x^3 y}{6} + \frac{L_D p_y x y^3}{6} + \frac{x^5}{24} + \frac{x^3 y^2}{12} + \frac{x y^4}{24} \end{pmatrix} \right\} \text{decapolar-like} \tag{B.15}$$

B

B.2.4. Transfer Map of a Skew Quadrupole and Octupole

The transfer map of a skew quadrupole H_1 and octupole H_2 of strength K_1 and K_2, separated by a drift like in the previous examples is given by

$$\mathcal{M} = e^{:Z:} = e^{:H_2:} \cdot e^{D:H_1:} \tag{B.16}$$

with H_1 and H_2 having as final expressions,

$$\begin{aligned} H_1 &= -J_1 L_1 \left(L_D p_x + x\right) \left(L_D p_y + y\right) \\ H_2 &= \frac{1}{4!} K_2 L_2 \left(x^4 - 6x^2 y^2 + y^4\right). \end{aligned} \tag{B.17}$$

The first two orders of the BCH of those two elements is given below.

First Order

$$\begin{aligned} &J_1 L_1 \left(-L_D^2 p_x p_y - L_D p_x y - L_D p_y x - xy\right) \Big\} \text{ skew quadrupolar} \\ &+K_2 L_2 \left(\frac{x^4}{24} - \frac{x^2 y^2}{4} + \frac{y^4}{24}\right) \Big\} \text{ octupolar} \end{aligned} \tag{B.18}$$

Second Order

$$J_1 K_2 L_1 L_2 L_D \left.\begin{pmatrix} \frac{L_D p_x x^2 y}{4} - \frac{L_D p_x y^3}{12} - \frac{L_D p_y x^3}{12} \\ + \frac{L_D p_y x y^2}{4} + \frac{x^3 y}{6} + \frac{x y^3}{6} \end{pmatrix}\right\} \text{ skew octupolar-like} \tag{B.19}$$

B

C

Chromatic Amplitude Detuning

This appendix details the derivations of chromatic amplitude detuning from sextupoles up to dodecapoles. As chromaticity and amplitude detuning are part of it, they will therefore be detailed here as well.

Up to the third order, the expression of the Taylor expansion of the Chromatic Amplitude Detuning around ϵ_x, ϵ_y and δ, for a tune Q_z, $z \in \{x, y\}$ reads:

$$
\begin{aligned}
Q_z(\epsilon_x, \epsilon_y, \delta) = Q_{z0} &+ \left[\frac{\partial Q_z}{\partial \epsilon_x}\epsilon_x + \frac{\partial Q_z}{\partial \epsilon_y}\epsilon_y + \frac{\partial Q_z}{\partial \delta}\delta\right] \\
&+ \frac{1}{2!}\left[\frac{\partial^2 Q_z}{\partial \epsilon_x^2}\epsilon_x^2 + \frac{\partial^2 Q_z}{\partial \epsilon_y^2}\epsilon_y^2 + \frac{\partial^2 Q_z}{\partial \delta^2}\delta^2\right. \\
&\qquad \left. + 2\frac{\partial^2 Q_z}{\partial \epsilon_x \partial \epsilon_y}\epsilon_x\epsilon_y + 2\frac{\partial^2 Q_z}{\partial \epsilon_x \partial \delta}\epsilon_x\delta + 2\frac{\partial^2 Q_z}{\partial \delta \partial \epsilon_y}\delta\epsilon_y\right] \\
&+ \frac{1}{3!}\left[\frac{\partial^3 Q_z}{\partial \delta^3}\delta^3 + \frac{\partial^3 Q_z}{\partial \epsilon_x^3}\epsilon_x^3 + \frac{\partial^3 Q_z}{\partial \epsilon_y^3}\epsilon_y^3\right. \\
&\qquad + 3\frac{\partial^3 Q_z}{\partial \epsilon_x \partial \delta^2}\delta^2\epsilon_x + 3\frac{\partial^3 Q_z}{\partial \epsilon_y \partial \delta^2}\delta^2\epsilon_y + 3\frac{\partial^3 Q_z}{\partial \epsilon_x^2 \partial \delta}\delta\epsilon_x^2 \\
&\qquad + 3\frac{\partial^3 Q_z}{\partial \epsilon_y^2 \partial \delta}\delta\epsilon_y^2 + 3\frac{\partial^3 Q_z}{\partial \epsilon_y \partial \epsilon_x^2}\epsilon_x^2\epsilon_y + 3\frac{\partial^3 Q_z}{\partial \epsilon_y^2 \partial \epsilon_x}\epsilon_x\epsilon_y^2 \\
&\qquad \left. + 6\frac{\partial^3 Q_z}{\partial \epsilon_y \partial \epsilon_x \partial \delta}\delta\epsilon_x\epsilon_y\right] + \cdots
\end{aligned}
\tag{C.1}
$$

C.1. Principle

From [15], the detuning caused by a magnet of length L can be described by its hamiltonian with

$$
\Delta Q_z = \frac{1}{2\pi}\int_L \frac{\partial \langle H \rangle}{\partial J_z}\,\mathrm{d}s. \tag{C.2}
$$

The usual variables x and y of Eq. (2.7) can be replaced by *action-angle* variables to introduce the action:

$$
\begin{aligned}
x &\longrightarrow \sqrt{2J_x\beta_x}\cos\phi_x \\
y &\longrightarrow \sqrt{2J_y\beta_y}\cos\phi_x
\end{aligned}
\tag{C.3}
$$

A momentum dependence can be introduced for a particle with a different orbit (Δz) [31] via dispersion. Combined with Eq. (C.3), a dependence on all required components is achieved:

$$
\begin{aligned}
x + \Delta x &\longrightarrow \sqrt{2J_x\beta_x}\cos\phi_x + D_x\delta \\
y + \Delta y &\longrightarrow \sqrt{2J_y\beta_y}\cos\phi_y + D_y\delta
\end{aligned}
\tag{C.4}
$$

After averaging over the phase variable, all that is left is to compute the partial derivatives.

The following derivations are just copy-paster from old text

C.2. Sextupole

The change of tune induced by a sextupole is:

$$Q_x = \frac{1}{4\pi}K_3\beta_x\eta\delta L \tag{C.5}$$

$$Q_y = -\frac{1}{4\pi}K_3\beta_y\eta\delta L \tag{C.6}$$

We can now get the terms we're interested in:

$$
\begin{aligned}
\frac{\partial Q_x}{\partial J_x} = 0 \quad &; \quad \frac{\partial Q_x}{\partial J_y} = 0 \quad ; \quad \frac{\partial Q_x}{\partial \delta} = \frac{1}{4\pi}K_3\beta_x\eta L = Q'_x \\
\frac{\partial Q_y}{\partial J_x} = 0 \quad &; \quad \frac{\partial Q_y}{\partial J_y} = 0 \quad ; \quad \frac{\partial Q_y}{\partial \delta} = -\frac{1}{4\pi}K_3\beta_y\eta L = Q'_y
\end{aligned}
\tag{C.7}
$$

C

Contribution to the Chromatic Amplitude Detuning:

$$Q_z(\epsilon_x, \epsilon_y, \delta) = Q_{z0} + \left[\frac{\partial Q_z}{\partial \epsilon_x} \epsilon_x + \frac{\partial Q_z}{\partial \epsilon_y} \epsilon_y + \frac{\partial Q_z}{\partial \delta} \delta \right] \tag{C.8}$$

C

C.2.1. Octupole

From the hamiltonian of a normal octupole, with a displacement in x (??), we can change the variable ($x = \sqrt{2J_x\beta_x}\cos\phi_x$ and $y = \sqrt{2J_y\beta_y}\cos\phi_y$):

$$
\begin{aligned}
\mathcal{N}_4 = \frac{1}{24}K_4\Bigg[& \left(\sqrt{2J_x\beta_x} cos\phi_x\right)^4 \\
& + 4\left(\sqrt{2J_x\beta_x}\cos\phi_x\right)^3 \eta\delta \\
& + 6\left(\sqrt{2J_x\beta_x}\cos\phi_x\right)^2 \eta^2\delta^2 \\
& + 4\left(\sqrt{2J_x\beta_x}\cos\phi_x\right) \eta^2\delta \\
& + \eta^4\delta^4 \\
& - 6\left(\sqrt{2J_x\beta_x}\cos\phi_x\right)^2 \left(\sqrt{2J_y\beta_y}\cos\phi_y\right)^2 \\
& - 6\left(\sqrt{2J_y\beta_y}\cos\phi_y\right)^2 \cdot 2\left(\sqrt{2J_x\beta_x}\cos\phi_x\right)\eta\delta \\
& - 6\left(\sqrt{2J_y\beta_y}\cos\phi_y\right)^2 \eta^2\delta^2 \\
& + \left(\sqrt{2J_y\beta_y}\cos\phi_y\right)^4\Bigg]
\end{aligned}
\tag{C.9}
$$

We can now average over the phase variables:

$$\begin{aligned}\langle \mathcal{N}_4 \rangle = \frac{1}{24} K_4 \bigg[& \frac{3}{2} J_x^2 \beta_x^2 \\ & + 6 J_x \beta_x \eta^2 \delta^2 \\ & + \eta^4 \delta^4 \\ & - 6 J_x \beta_x J_y \beta_y \\ & - 6 J_y \beta_y \eta^2 \delta^2 \\ & + \frac{3}{2} J_y^2 \beta_y^2 \bigg]\end{aligned} \tag{C.10}$$

The tunes then are:

$$\begin{aligned} Q_x &= \frac{1}{2\pi} \frac{\partial \langle \mathcal{N}_\triangle \rangle}{\partial J_x} = \frac{1}{48\pi} K_4 \left[3 J_x \beta_x^2 + 6 \beta_x \eta^2 \delta^2 - 6 \beta_x J_y \beta_y \right] \\ Q_y &= \frac{1}{2\pi} \frac{\partial \langle \mathcal{N}_\triangle \rangle}{\partial J_y} = \frac{1}{48\pi} K_4 \left[-6 J_x \beta_x \beta_y - 6 \beta_y \eta^2 \delta^2 + 3 J_y \beta_y^2 \right] \end{aligned} \tag{C.11}$$

$$\begin{aligned} &\frac{\partial Q_x}{\partial J_x} = \frac{1}{16\pi} K_4 \beta_x^2 \quad ; \quad \frac{\partial Q_x}{\partial J_y} = -\frac{1}{8\pi} K_4 \beta_x \beta_y \quad ; \quad \frac{\partial^2 Q_x}{\partial \delta^2} = \frac{1}{4\pi} K_4 \beta_x \eta^2 = Q_x'' \\ &\frac{\partial Q_y}{\partial J_x} = -\frac{1}{8\pi} K_4 \beta_x \beta_y \quad ; \quad \frac{\partial Q_y}{\partial J_y} = \frac{1}{16\pi} K_4 \beta_y^2 \quad ; \quad \frac{\partial^2 Q_y}{\partial \delta^2} = -\frac{1}{4\pi} K_4 \beta_y \eta^2 = Q_y'' \end{aligned} \tag{C.12}$$

Contribution to the Chromatic Amplitude Detuning:

C

$$
\begin{aligned}
Q_z(\epsilon_x, \epsilon_y, \delta) = Q_{z0} &+ \left[\frac{\partial Q_z}{\partial \epsilon_x}\epsilon_x + \frac{\partial Q_z}{\partial \epsilon_y}\epsilon_y + \frac{\partial Q_z}{\partial \delta}\delta\right] \\
&+ \frac{1}{2!}\left[\frac{\partial^2 Q_z}{\partial \epsilon_x^2}\epsilon_x^2 + \frac{\partial^2 Q_z}{\partial \epsilon_y^2}\epsilon_y^2 + \frac{\partial^2 Q_z}{\partial \delta^2}\delta^2\right. \\
&\qquad \left. + 2\frac{\partial^2 Q_z}{\partial \epsilon_x \partial \epsilon_y}\epsilon_x\epsilon_y + 2\frac{\partial^2 Q_z}{\partial \epsilon_x \partial \delta}\epsilon_x\delta + 2\frac{\partial^2 Q_z}{\partial \delta \partial \epsilon_y}\delta\epsilon_y\right] \\
&+ \frac{1}{3!}\left[\frac{\partial^3 Q_z}{\partial \delta^3}\delta^3 + \frac{\partial^3 Q_z}{\partial \epsilon_x^3}\epsilon_x^3 + \frac{\partial^3 Q_z}{\partial \epsilon_y^3}\epsilon_y^3\right. \\
&\qquad + 3\frac{\partial^3 Q_z}{\partial \epsilon_x \partial \delta^2}\delta^2\epsilon_x + 3\frac{\partial^3 Q_z}{\partial \epsilon_y \partial \delta^2}\delta^2\epsilon_y + 3\frac{\partial^3 Q_z}{\partial \epsilon_x^2 \partial \delta}\delta\epsilon_x^2 \\
&\qquad + 3\frac{\partial^3 Q_z}{\partial \epsilon_y^2 \partial \delta}\delta\epsilon_y^2 + 3\frac{\partial^3 Q_z}{\partial \epsilon_y \partial \epsilon_x^2}\epsilon_x^2\epsilon_y + 3\frac{\partial^3 Q_z}{\partial \epsilon_y^2 \partial \epsilon_x}\epsilon_x\epsilon_y^2 \\
&\qquad \left. + 6\frac{\partial^3 Q_z}{\partial \epsilon_y \partial \epsilon_x \partial \delta}\delta\epsilon_x\epsilon_y\right]
\end{aligned} \tag{C.13}
$$

C

C.2.2. Decapole

The normal field of a decapole has been calculated in ??:

$$
\begin{aligned}
\mathcal{N}_{\triangledown}(x,y) = \frac{1}{120}K_5 \Big[& \eta^5\delta^5 + 5\eta^4\delta^4 x + 10\eta^3\delta^3 x^2 + 10\eta^2\delta^2 x^3 + 5\eta\delta x^4 + x^5 \\
& - 10y^2(\eta^3\delta^3 + 3\eta^2\delta^2 x + 3\eta\delta x^2 + x^3) \\
& + 5y^4(x+\eta\delta) \Big]
\end{aligned}
$$

Changing variables ($x \longrightarrow \sqrt{2J_x\beta_x}\cos\phi_x$; $y \longrightarrow \sqrt{2J_y\beta_y}\cos\phi_y$):

$$
\begin{aligned}
\mathcal{N}_{\triangledown}(x,y) = \frac{1}{120}K_5 \Big[& \eta^5\delta^5 + 5\eta^4\delta^4 \left(\sqrt{2J_x\beta_x}\cos\phi_x\right) \\
& + 10\eta^3\delta^3 \left(\sqrt{2J_x\beta_x}\cos\phi_x\right)^2 + 10\eta^2\delta^2 \left(\sqrt{2J_x\beta_x}\cos\phi_x\right)^3 \\
& + 5\eta\delta \left(\sqrt{2J_x\beta_x}\cos\phi_x\right)^4 + \left(\sqrt{2J_x\beta_x}\cos\phi_x\right)^5 \\
& - 10 \left(\sqrt{2J_y\beta_y}\cos\phi_y\right)^2 \Big[(\eta^3\delta^3 + 3\eta^2\delta^2 \left(\sqrt{2J_x\beta_x}\cos\phi_x\right) \\
& \qquad + 3\eta\delta \left(\sqrt{2J_x\beta_x}\cos\phi_x\right)^2 + \left(\sqrt{2J_x\beta_x}\cos\phi_x\right)^3 \Big] \\
& + 5 \left(\sqrt{2J_y\beta_y}\cos\phi_y\right)^4 \left(\left(\sqrt{2J_x\beta_x}\cos\phi_x\right) + \eta\delta \right) \Big]
\end{aligned}
\tag{C.14}
$$

C

Averaging over the phase variables:

$$\begin{aligned}\mathcal{N}_{\triangledown}(x,y) = \frac{1}{120}K_5\Bigg[&\eta^5\delta^5 + 10\eta^3\delta^3 J_x\beta_x \\ &+ \frac{15}{2}\eta\delta J_x^2\beta_x^2 - 10J_y\beta_y\eta^3\delta^3 \\ &- 30J_y\beta_y\eta\delta J_x\beta_x + \frac{15}{2}J_y^2\beta_y^2\eta\delta\Bigg]\end{aligned} \tag{C.15}$$

The tunes then are:

$$\begin{aligned}Q_x &= \frac{1}{2\pi}\frac{\partial\langle\mathcal{N}_{\triangledown}\rangle}{\partial J_x} = \frac{1}{240\pi}K_5\left[10\eta^3\delta^3\beta_x + 15\eta\delta J_x\beta_x^2 - 30J_y\beta_y\beta_x\eta\delta\right] \\ Q_y &= \frac{1}{2\pi}\frac{\partial\langle\mathcal{N}_{\triangledown}\rangle}{\partial J_y} = \frac{1}{240\pi}K_5\left[-10\eta^3\delta^3\beta_y + 15\eta\delta J_y\beta_y^2 - 30J_x\beta_y\beta_x\eta\delta\right]\end{aligned} \tag{C.16}$$

We can now calculate our chromatic amplitude detuning terms:

$$\begin{aligned}\frac{\partial^2 Q_x}{\partial J_x\partial\delta} &= \frac{1}{16\pi}K_5\beta_x^2\eta \quad ; \quad \frac{\partial^2 Q_x}{\partial J_y\partial\delta} = -\frac{1}{8\pi}K_5\beta_x\beta_y\eta \quad ; \quad \frac{\partial^3 Q_x}{\partial\delta^3} = \frac{1}{4\pi}K_5\beta_x\eta^3 = Q_x''' \\ \frac{\partial^2 Q_y}{\partial J_x\partial\delta} &= -\frac{1}{8\pi}K_5\beta_x\beta_y\eta \quad ; \quad \frac{\partial^2 Q_y}{\partial J_y\partial\delta} = \frac{1}{16\pi}K_5\beta_y^2\eta \quad ; \quad \frac{\partial^3 Q_y}{\partial\delta^3} = -\frac{1}{4\pi}K_5\beta_y\eta^3 = Q_y'''\end{aligned} \tag{C.17}$$

Contribution to the Chromatic Amplitude Detuning:

C

$$
\begin{aligned}
Q_z(\epsilon_x, \epsilon_y, \delta) = Q_{z0} &+ \left[\frac{\partial Q_z}{\partial \epsilon_x}\epsilon_x + \frac{\partial Q_z}{\partial \epsilon_y}\epsilon_y + \frac{\partial Q_z}{\partial \delta}\delta\right] \\
&+ \frac{1}{2!}\left[\frac{\partial^2 Q_z}{\partial \epsilon_x^2}\epsilon_x^2 + \frac{\partial^2 Q_z}{\partial \epsilon_y^2}\epsilon_y^2 + \frac{\partial^2 Q_z}{\partial \delta^2}\delta^2\right. \\
&\qquad \left. + 2\frac{\partial^2 Q_z}{\partial \epsilon_x \partial \epsilon_y}\epsilon_x\epsilon_y + 2\frac{\partial^2 Q_z}{\partial \epsilon_x \partial \delta}\epsilon_x\delta + 2\frac{\partial^2 Q_z}{\partial \delta \partial \epsilon_y}\delta\epsilon_y\right] \\
&+ \frac{1}{3!}\left[\frac{\partial^3 Q_z}{\partial \delta^3}\delta^3 + \frac{\partial^3 Q_z}{\partial \epsilon_x^3}\epsilon_x^3 + \frac{\partial^3 Q_z}{\partial \epsilon_y^3}\epsilon_y^3\right. \\
&\qquad + 3\frac{\partial^3 Q_z}{\partial \epsilon_x \partial \delta^2}\delta^2\epsilon_x + 3\frac{\partial^3 Q_z}{\partial \epsilon_y \partial \delta^2}\delta^2\epsilon_y + 3\frac{\partial^3 Q_z}{\partial \epsilon_x^2 \partial \delta}\delta\epsilon_x^2 \\
&\qquad + 3\frac{\partial^3 Q_z}{\partial \epsilon_y^2 \partial \delta}\delta\epsilon_y^2 + 3\frac{\partial^3 Q_z}{\partial \epsilon_y \partial \epsilon_x^2}\epsilon_x^2\epsilon_y + 3\frac{\partial^3 Q_z}{\partial \epsilon_y^2 \partial \epsilon_x}\epsilon_x\epsilon_y^2 \\
&\qquad \left. + 6\frac{\partial^3 Q_z}{\partial \epsilon_y \partial \epsilon_x \partial \delta}\delta\epsilon_x\epsilon_y\right]
\end{aligned} \tag{C.18}
$$

C

C.2.3. Dodecapole

The main normal field of a dodecapole is:

$$\mathcal{N}(x,y) = \frac{1}{720} K_6 (x^6 - 15x^4y^2 + 15x^2y^4 - y^6) \tag{C.19}$$

With a displacement in $x \longrightarrow x + \eta\delta$:

$$\mathcal{N}(x,y) = \frac{1}{720} K_6 \left[(x+\eta\delta)^6 - 15(x+\eta\delta)^4 y^2 + 15(x+\eta\delta)^2 y^4 - y^6 \right] \tag{C.20}$$

Expanded form, after having removed odd exponents. Those exponents would yield an average of 0 for the cosines:

$$\begin{aligned}\mathcal{N}(x,y) = \frac{1}{720} K_6 \Big[& x^6 + 15x^2\eta^4\delta^4 + 15x^4\eta^2\delta^2 + \eta^6\delta^6 \\ & - 15y^2(\eta^4\delta^4 + 4x\eta^3\delta^3 + 6x^2\eta^2\delta^2 + 4x^3\eta\delta + x^4) \\ & + 15y^4(x^2 + \eta^2\delta^2) \\ & - y^6 \Big]\end{aligned} \tag{C.21}$$

C

Changing variables ($x \to \sqrt{2J_x\beta_x}\cos\phi_x$; $y \to \sqrt{2J_y\beta_y}\cos\phi_y$):

$$
\begin{aligned}
\mathcal{N}(x,y) = \frac{1}{720}K_6\Bigg[& \left(\sqrt{2J_x\beta_x}\cos\phi_x\right)^6 \\
& + 15\left(\sqrt{2J_x\beta_x}\cos\phi_x\right)^2\eta^4\delta^4 \\
& + 15\left(\sqrt{2J_x\beta_x}\cos\phi_x\right)^4\eta^2\delta^2 \\
& + \eta^6\delta^6 \\
& - 15\left(\sqrt{2J_y\beta_y}\cos\phi_y\right)^2\Bigg(\eta^4\delta^4 \\
& \qquad + 6\left(\sqrt{2J_x\beta_x}\cos\phi_x\right)^2\eta^2\delta^2 \\
& \qquad + \left(\sqrt{2J_x\beta_x}\cos\phi_x\right)^4\Bigg) \\
& + 15\left(\sqrt{2J_y\beta_y}\cos\phi_y\right)^4\left(\left(\sqrt{2J_x\beta_x}\cos\phi_x\right)^2 + \eta^2\delta^2\right) \\
& - \left(\sqrt{2J_y\beta_y}\cos\phi_y\right)^6\Bigg]
\end{aligned}
\tag{C.22}
$$

C

Averaging over the phase variables:

$$
\begin{aligned}
\left\langle \mathcal{N}(x,y) \right\rangle = \frac{1}{720} K_6 \Bigg[& \frac{5}{2} J_x^3 \beta_x^3 \\
& + 15 \cdot J_x \beta_x \eta^4 \delta^4 \\
& + 15 \cdot J_x^2 \beta_x^2 \frac{3}{2} \eta^2 \delta^2 \\
& + \eta^6 \delta^6 \\
& - 15 \left(J_y \beta_y \right) \Bigg(\eta^4 \delta^4 \\
& \qquad + 6 \left(J_x \beta_x \right) \eta^2 \delta^2 \\
& \qquad + \left(J_x^2 \beta_x^2 \frac{3}{2} \right) \Bigg) \\
& + 15 \left(J_y^2 \beta_y^2 \frac{3}{2} \right) \left(J_x \beta_x + \eta^2 \delta^2 \right) \\
& - \frac{5}{2} J_y^3 \beta_y^3 \Bigg]
\end{aligned}
\tag{C.23}
$$

The tunes then are:

C

$$
\begin{aligned}
Q_x = \frac{1}{2\pi}\frac{\partial \left\langle \mathcal{N} \right\rangle}{\partial J_x} = \frac{1}{1440\pi} K_6 \Bigg[& \frac{15}{2} J_x^2 \beta_x^3 \\
& + 15 \beta_x \eta^4 \delta^4 \\
& + 45 J_x \beta_x^2 \eta^2 \delta^2 \\
& - 90 J_y \beta_y \beta_x \eta^2 \delta^2 \\
& - 45 J_y \beta_y J_x \beta_x^2 \\
& + 15 \cdot \frac{3}{2} J_y^2 \beta_y^2 \beta_x \Bigg] \\
Q_y = \frac{1}{2\pi}\frac{\partial \left\langle \mathcal{N} \right\rangle}{\partial J_y} = \frac{1}{1440\pi} K_6 \Bigg[& -15 \beta_y \eta^4 \delta^4 \\
& - 90 \beta_y J_x \beta_x \eta^2 \delta^2 \\
& - 15 \cdot \frac{3}{2} \beta_y J_x^2 \beta_x^2 \\
& + 45 J_y \beta_y^2 J_x \beta_x \\
& + 45 J_y \beta_y^2 \eta^2 \delta^2 \\
& - \frac{15}{2} J_y^2 \beta_y^3 \Bigg]
\end{aligned}
\tag{C.24}
$$

We can now calculate our chromatic amplitude detuning terms. Since there are many terms, I'm going to split them here. First, Q_x:

C

$$\begin{aligned}
\frac{\partial^2 Q_x}{\partial J_x^2} &= \frac{1}{96\pi} K_6 \beta_x^3 \\
\frac{\partial^3 Q_x}{\partial J_x \partial \delta^2} &= \frac{1}{16\pi} K_6 \beta_x^2 \eta^2 \\
\hline
\frac{\partial^2 Q_x}{\partial J_y^2} &= \frac{1}{32\pi} K_6 \beta_y^2 \beta_x \\
\frac{\partial^3 Q_x}{\partial J_y \partial \delta^2} &= -\frac{1}{8\pi} K_6 \beta_y \beta_x \eta^2 \\
\hline
\frac{\partial^2 Q_x}{\partial J_x \partial J_y} &= -\frac{1}{32\pi} K_6 \beta_y \beta_x^2
\end{aligned} \tag{C.25}$$

Then Q_y:

$$\begin{aligned}
\frac{\partial^2 Q_y}{\partial J_y^2} &= -\frac{1}{96\pi} K_6 \beta_y^3 \\
\frac{\partial^3 Q_y}{\partial J_y \partial \delta^2} &= \frac{1}{16\pi} K_6 \beta_y^2 \eta^2 \\
\hline
\frac{\partial^2 Q_y}{\partial J_x^2} &= -\frac{1}{32\pi} K_6 \beta_y \beta_x^2 \\
\frac{\partial^3 Q_y}{\partial J_x \partial \delta^2} &= -\frac{1}{8\pi} K_6 \beta_y \beta_x \eta^2 \\
\hline
\frac{\partial^2 Q_y}{\partial J_y \partial J_x} &= \frac{1}{32\pi} K_6 \beta_y^2 \beta_x
\end{aligned} \tag{C.26}$$

C

Then the chromaticity:

$$\begin{aligned} \frac{\partial^4 Q_x}{\partial \delta^4} &= \frac{1}{4\pi} K_6 \beta_x \eta^4 = Q_x'''' \\ \frac{\partial^4 Q_y}{\partial \delta^4} &= -\frac{1}{4\pi} K_6 \beta_y \eta^4 = Q_y'''' \end{aligned} \tag{C.27}$$

Contribution to the Chromatic Amplitude Detuning:

$$\begin{aligned} Q_z(\epsilon_x, \epsilon_y, \delta) = Q_{z0} &+ \left[\frac{\partial Q_z}{\partial \epsilon_x} \epsilon_x + \frac{\partial Q_z}{\partial \epsilon_y} \epsilon_y + \frac{\partial Q_z}{\partial \delta} \delta \right] \\ &+ \frac{1}{2!} \left[\frac{\partial^2 Q_z}{\partial \epsilon_x^2} \epsilon_x^2 + \frac{\partial^2 Q_z}{\partial \epsilon_y^2} \epsilon_y^2 + \frac{\partial^2 Q_z}{\partial \delta^2} \delta^2 \right. \\ &\qquad \left. + 2 \frac{\partial^2 Q_z}{\partial \epsilon_x \partial \epsilon_y} \epsilon_x \epsilon_y + 2 \frac{\partial^2 Q_z}{\partial \epsilon_x \partial \delta} \epsilon_x \delta + 2 \frac{\partial^2 Q_z}{\partial \delta \partial \epsilon_y} \delta \epsilon_y \right] \\ &+ \frac{1}{3!} \left[\frac{\partial^3 Q_z}{\partial \delta^3} \delta^3 + \frac{\partial^3 Q_z}{\partial \epsilon_x^3} \epsilon_x^3 + \frac{\partial^3 Q_z}{\partial \epsilon_y^3} \epsilon_y^3 \right. \\ &\qquad + 3 \frac{\partial^3 Q_z}{\partial \epsilon_x \partial \delta^2} \delta^2 \epsilon_x + 3 \frac{\partial^3 Q_z}{\partial \epsilon_y \partial \delta^2} \delta^2 \epsilon_y + 3 \frac{\partial^3 Q_z}{\partial \epsilon_x^2 \partial \delta} \delta \epsilon_x^2 \\ &\qquad + 3 \frac{\partial^3 Q_z}{\partial \epsilon_y^2 \partial \delta} \delta \epsilon_y^2 + 3 \frac{\partial^3 Q_z}{\partial \epsilon_y \partial \epsilon_x^2} \epsilon_x^2 \epsilon_y + 3 \frac{\partial^3 Q_z}{\partial \epsilon_y^2 \partial \epsilon_x} \epsilon_x \epsilon_y^2 \\ &\qquad \left. + 6 \frac{\partial^3 Q_z}{\partial \epsilon_y \partial \epsilon_x \partial \delta} \delta \epsilon_x \epsilon_y \right] \\ &+ \frac{1}{4!} \left[\frac{\partial^4 Q_z}{\partial \delta^4} \delta^4 \right] \end{aligned} \tag{C.28}$$

C.2.4. PTC check

A simulation has been done with PTC to assess that those equations are correct. A dodecapole has been added to the lattice with a strength $KL = 1e^6$. Here are the results, confirming PTC works as intended.

The ANH numbers refer to the partial derivative relative to J_x, J_y and δ. So ANHX 021 would for example be $\dfrac{\partial^3 Q_x}{\partial J_y^2 \partial\delta}$.

Term	Analytical	Simulation	Rel. Diff [%]
ANH X 200	4782639.96971	4782639.97	0.0
ANH X 102	86945.930342	86945.93	-0.0
ANH X 020	593469879.552116	593469880.01	0.0
ANH X 012	-1118366.433407	-1118366.433	-0.0
ANH X 110	-92277073.535598	-92277073.6	0.0
ANH X 004	1053.754809	1053.7548	-0.000001
ANH Y 200	-92277073.535598	-92277073.6	0.0
ANH Y 102	-1118366.433407	-1118366.433	-0.0
ANH Y 020	-1272278817.264865	-1272278818.913	0.0
ANH Y 012	3596325.539479	3596325.543	0.0
ANH Y 110	593469879.552116	593469880.01	0.0
ANH Y 004	-6777.108503	-6777.1085	-0.0

C

D

Resonance Driving Terms

derivations
plots of phase spaces

This appendix intends to clarify where Resonance Driving Terms can be seen in the frequency spectrum, what resonance they contribute to and what their action dependance is. The number of valid RDTs indeed grows rapidly with the magnet order n, as shows Table D.1, and is given by the following combinations:

$$C(n+3,3) - C(n+1,1) - [(n+1) \bmod 2] \cdot C\left(\left\lfloor \frac{n}{2} \right\rfloor + 1, 1\right). \tag{D.1}$$

D

Multipole	Order	Number of poles	Number of RDTs
Quadrupole	2	4	5
Sextupole	3	6	16
Octupole	4	8	27
Decapole	5	10	50
Dodecapole	6	12	73
Decatetrapole	7	14	112
Decahexapole	8	16	151
Hectopole	50	100	23349
Kilopole	500	1000	2.1×10^7

Table D.1.: Number of valid RDTs for a given multipole order

Several different RDTs can contribute to the same line, which can be observed in the horizontal or vertical spectrum. The tables below describe which RDTs contribute to a specific combination of line and plane. All tables have been computed up to the order 6, for decapoles. The line columns represents (Q_x, Q_y). For example (-1, 2) is $-1Q_x + 2Qy$.

As a reminder, for a given RDT f_{jklm}, we will observe:

$$\begin{aligned} &(j-k)Q_x + (l-m)Q_y = p \in \mathbb{N} && \text{excited resonance} \\ &H(1-j+k, m-l) && \text{horizontal line, if } j \neq 0 \\ &V(k-j, 1-l+m) && \text{vertical line, if } l \neq 0. \end{aligned} \tag{D.2}$$

The amplitude of each line is given by:

$$\begin{aligned} |H_{f_{jklm}}| &= 2j(2I_x)^{\frac{j+k-1}{2}}(2I_y)^{\frac{l+m}{2}}|f_{jklm}| \\ |V_{f_{jklm}}| &= 2l(2I_x)^{\frac{j+k}{2}}(2I_y)^{\frac{l+m-1}{2}}|f_{jklm}|. \end{aligned} \tag{D.3}$$

According to equations D.2 and D.3, it can be seen that many RDTs will no generate any line and thus can not be observed.

D.1. Frequency Spectrum Lines

D.1.1. Horizontal Axis

H-line	RDTs
(-5, 0)	f6000
(-4, -1)	f5010
(-4, 0)	f5000
(-4, 1)	f5001
(-3, -2)	f4020
(-3, -1)	f4010
(-3, 0)	f4000, f4011, f5100
(-3, 1)	f4001
(-3, 2)	f4002
(-2, -3)	f3030
(-2, -2)	f3020
(-2, -1)	f3010, f3021, f4110
(-2, 0)	f3000, f3011, f4100
(-2, 1)	f3001, f3012, f4101
(-2, 2)	f3002
(-2, 3)	f3003
(-1, -4)	f2040
(-1, -3)	f2030
(-1, -2)	f2020, f2031, f3120
(-1, -1)	f2010, f2021, f3110
(-1, 0)	f2000, f2011, f3100, f2022, f3111, f4200
(-1, 1)	f2001, f2012, f3101
(-1, 2)	f2002, f2013, f3102
(-1, 3)	f2003
(-1, 4)	f2004
(0, -5)	f1050

D

H-line	RDTs
(0, -4)	f1040
(0, -3)	f1030, f1041, f2130
(0, -2)	f1020, f1031, f2120
(0, -1)	f1010, f1021, f2110, f1032, f2121, f3210
(0, 0)	f1011, f2100, f1022, f2111, f3200
(0, 1)	f1001, f1012, f2101, f1023, f2112, f3201
(0, 2)	f1002, f1013, f2102
(0, 3)	f1003, f1014, f2103
(0, 4)	f1004
(0, 5)	f1005
(1, -4)	f1140
(1, -3)	f1130
(1, -2)	f1120, f1131, f2220
(1, -1)	f1110, f1121, f2210
(1, 1)	f1101, f1112, f2201
(1, 2)	f1102, f1113, f2202
(1, 3)	f1103
(1, 4)	f1104
(2, -3)	f1230
(2, -2)	f1220
(2, -1)	f1210, f1221, f2310
(2, 0)	f1200, f1211, f2300
(2, 1)	f1201, f1212, f2301
(2, 2)	f1202
(2, 3)	f1203
(3, -2)	f1320
(3, -1)	f1310
(3, 0)	f1300, f1311, f2400
(3, 1)	f1301
(3, 2)	f1302

H-line	RDTs
(4, -1)	f1410
(4, 0)	f1400
(4, 1)	f1401
(5, 0)	f1500

D.1.2. Vertical Axis

V-line	RDTs
(-5, 0)	f5010
(-4, -1)	f4020
(-4, 0)	f4010
(-4, 1)	f4011
(-3, -2)	f3030
(-3, -1)	f3020
(-3, 0)	f3010, f3021, f4110
(-3, 1)	f3011
(-3, 2)	f3012
(-2, -3)	f2040
(-2, -2)	f2030
(-2, -1)	f2020, f2031, f3120
(-2, 0)	f2010, f2021, f3110
(-2, 1)	f2011, f2022, f3111
(-2, 2)	f2012
(-2, 3)	f2013
(-1, -4)	f1050
(-1, -3)	f1040
(-1, -2)	f1030, f1041, f2130
(-1, -1)	f1020, f1031, f2120

V-line	RDTs
(-1, 0)	f1010, f1021, f2110, f1032, f2121, f3210
(-1, 1)	f1011, f1022, f2111
(-1, 2)	f1012, f1023, f2112
(-1, 3)	f1013
(-1, 4)	f1014
(0, -5)	f0060
(0, -4)	f0050
(0, -3)	f0040, f0051, f1140
(0, -2)	f0030, f0041, f1130
(0, -1)	f0020, f0031, f1120, f0042, f1131, f2220
(0, 0)	f0021, f1110, f0032, f1121, f2210
(0, 2)	f0012, f0023, f1112
(0, 3)	f0013, f0024, f1113
(0, 4)	f0014
(0, 5)	f0015
(1, -4)	f0150
(1, -3)	f0140
(1, -2)	f0130, f0141, f1230
(1, -1)	f0120, f0131, f1220
(1, 0)	f0110, f0121, f1210, f0132, f1221, f2310
(1, 1)	f0111, f0122, f1211
(1, 2)	f0112, f0123, f1212
(1, 3)	f0113
(1, 4)	f0114
(2, -3)	f0240
(2, -2)	f0230
(2, -1)	f0220, f0231, f1320
(2, 0)	f0210, f0221, f1310
(2, 1)	f0211, f0222, f1311
(2, 2)	f0212

V-line	RDTs
(2, 3)	f0213
(3, -2)	f0330
(3, -1)	f0320
(3, 0)	f0310, f0321, f1410
(3, 1)	f0311
(3, 2)	f0312
(4, -1)	f0420
(4, 0)	f0410
(4, 1)	f0411
(5, 0)	f0510

D.2. Amplitude, Resonances and Lines

This part focuses on individual Resonance Drivings Terms, expliciting what magnet they originate from, what resonance they excite, how they can be observed and what kicks are needed in order to measure them. The amplitude columns implicitly omits the term $|f_{jklm}|$, which depends on K and J.

Amplitude legend:

- I_x : depends only on horizontal amplitude
- I_y : depends only on vertical amplitude
- I_xI_y : depends on both horizontal and vertical amplitude

n	jklm	type	resonance	H-line	V-line	Amplitude H	Amplitude V
2	0020	normal	(0, 2)		(0, -1)		$4(2I_y)^{1/2}$
2	2000	normal	(2, 0)	(-1, 0)		$4(2I_x)^{1/2}$	
2	0110	skew	(-1, 1)		(1, 0)		$2(2I_x)^{1/2}$
2	1001	skew	(1, -1)	(0, 1)		$2(2I_y)^{1/2}$	
2	1010	skew	(1, 1)	(0, -1)	(-1, 0)	$2(2I_y)^{1/2}$	$2(2I_x)^{1/2}$
3	0111	normal	(-1, 0)		(1, 1)		$2(2I_x)^{1/2}(2I_y)^{1/2}$
3	0120	normal	(-1, 2)		(1, -1)		$4(2I_x)^{1/2}(2I_y)^{1/2}$
3	1002	normal	(1, -2)	(0, 2)		$2(2I_y)$	
3	1011	normal	(1, 0)	(0, 0)	(-1, 1)	$2(2I_y)$	$2(2I_x)^{1/2}(2I_y)^{1/2}$
3	1020	normal	(1, 2)	(0, -2)	(-1, -1)	$2(2I_y)$	$4(2I_x)^{1/2}(2I_y)^{1/2}$
3	1200	normal	(-1, 0)	(2, 0)		$2(2I_x)$	
3	2100	normal	(1, 0)	(0, 0)		$4(2I_x)$	
3	3000	normal	(3, 0)	(-2, 0)		$6(2I_x)$	
3	0012	skew	(0, -1)		(0, 2)		$2(2I_y)$
3	0021	skew	(0, 1)		(0, 0)		$4(2I_y)$
3	0030	skew	(0, 3)		(0, -2)		$6(2I_y)$
3	0210	skew	(-2, 1)		(2, 0)		$2(2I_x)$
3	1101	skew	(0, -1)	(1, 1)		$2(2I_x)^{1/2}(2I_y)^{1/2}$	

D

n	jklm	type	resonance	H-line	V-line	Amplitude H	Amplitude V
3	1110	skew	(0, 1)	(1, -1)	(0, 0)	$2(2I_x)^{1/2}(2I_y)^{1/2}$	$2(2I_x)$
3	2001	skew	(2, -1)	(-1, 1)		$4(2I_x)^{1/2}(2I_y)^{1/2}$	
3	2010	skew	(2, 1)	(-1, -1)	(-2, 0)	$4(2I_x)^{1/2}(2I_y)^{1/2}$	$2(2I_x)$
4	0013	normal	(0, -2)		(0, 3)		$2(2I_y)^{3/2}$
4	0031	normal	(0, 2)		(0, -1)		$6(2I_y)^{3/2}$
4	0040	normal	(0, 4)		(0, -3)		$8(2I_y)^{3/2}$
4	0211	normal	(-2, 0)		(2, 1)		$2(2I_x)(2I_y)^{1/2}$
4	0220	normal	(-2, 2)		(2, -1)		$4(2I_x)(2I_y)^{1/2}$
4	1102	normal	(0, -2)	(1, 2)		$2(2I_x)^{1/2}(2I_y)$	
4	1120	normal	(0, 2)	(1, -2)	(0, -1)	$2(2I_x)^{1/2}(2I_y)$	$4(2I_x)(2I_y)^{1/2}$
4	1300	normal	(-2, 0)	(3, 0)		$2(2I_x)^{3/2}$	
4	2002	normal	(2, -2)	(-1, 2)		$4(2I_x)^{1/2}(2I_y)$	
4	2011	normal	(2, 0)	(-1, 0)	(-2, 1)	$4(2I_x)^{1/2}(2I_y)$	$2(2I_x)(2I_y)^{1/2}$
4	2020	normal	(2, 2)	(-1, -2)	(-2, -1)	$4(2I_x)^{1/2}(2I_y)$	$4(2I_x)(2I_y)^{1/2}$
4	3100	normal	(2, 0)	(-1, 0)		$6(2I_x)^{3/2}$	
4	4000	normal	(4, 0)	(-3, 0)		$8(2I_x)^{3/2}$	
4	0112	skew	(-1, -1)		(1, 2)		$2(2I_x)^{1/2}(2I_y)$
4	0121	skew	(-1, 1)		(1, 0)		$4(2I_x)^{1/2}(2I_y)$
4	0130	skew	(-1, 3)		(1, -2)		$6(2I_x)^{1/2}(2I_y)$
4	0310	skew	(-3, 1)		(3, 0)		$2(2I_x)^{3/2}$
4	1003	skew	(1, -3)	(0, 3)		$2(2I_y)^{3/2}$	
4	1012	skew	(1, -1)	(0, 1)	(-1, 2)	$2(2I_y)^{3/2}$	$2(2I_x)^{1/2}(2I_y)$
4	1021	skew	(1, 1)	(0, -1)	(-1, 0)	$2(2I_y)^{3/2}$	$4(2I_x)^{1/2}(2I_y)$
4	1030	skew	(1, 3)	(0, -3)	(-1, -2)	$2(2I_y)^{3/2}$	$6(2I_x)^{1/2}(2I_y)$
4	1201	skew	(-1, -1)	(2, 1)		$2(2I_x)(2I_y)^{1/2}$	
4	1210	skew	(-1, 1)	(2, -1)	(1, 0)	$2(2I_x)(2I_y)^{1/2}$	$2(2I_x)^{3/2}$
4	2101	skew	(1, -1)	(0, 1)		$4(2I_x)(2I_y)^{1/2}$	
4	2110	skew	(1, 1)	(0, -1)	(-1, 0)	$4(2I_x)(2I_y)^{1/2}$	$2(2I_x)^{3/2}$

D

n	jklm	type	resonance	H-line	V-line	Amplitude H	Amplitude V
4	3001	skew	(3, -1)	(-2, 1)		$6(2I_x)(2I_y)^{1/2}$	
4	3010	skew	(3, 1)	(-2, -1)	(-3, 0)	$6(2I_x)(2I_y)^{1/2}$	$2(2I_x)^{3/2}$
5	0113	normal	(-1, -2)		(1, 3)		$2(2I_x)^{1/2}(2I_y)^{3/2}$
5	0122	normal	(-1, 0)		(1, 1)		$4(2I_x)^{1/2}(2I_y)^{3/2}$
5	0131	normal	(-1, 2)		(1, -1)		$6(2I_x)^{1/2}(2I_y)^{3/2}$
5	0140	normal	(-1, 4)		(1, -3)		$8(2I_x)^{1/2}(2I_y)^{3/2}$
5	0311	normal	(-3, 0)		(3, 1)		$2(2I_x)^{3/2}(2I_y)^{1/2}$
5	0320	normal	(-3, 2)		(3, -1)		$4(2I_x)^{3/2}(2I_y)^{1/2}$
5	1004	normal	(1, -4)	(0, 4)		$2(2I_y)^2$	
5	1013	normal	(1, -2)	(0, 2)	(-1, 3)	$2(2I_y)^2$	$2(2I_x)^{1/2}(2I_y)^{3/2}$
5	1022	normal	(1, 0)	(0, 0)	(-1, 1)	$2(2I_y)^2$	$4(2I_x)^{1/2}(2I_y)^{3/2}$
5	1031	normal	(1, 2)	(0, -2)	(-1, -1)	$2(2I_y)^2$	$6(2I_x)^{1/2}(2I_y)^{3/2}$
5	1040	normal	(1, 4)	(0, -4)	(-1, -3)	$2(2I_y)^2$	$8(2I_x)^{1/2}(2I_y)^{3/2}$
5	1202	normal	(-1, -2)	(2, 2)		$2(2I_x)(2I_y)$	
5	1211	normal	(-1, 0)	(2, 0)	(1, 1)	$2(2I_x)(2I_y)$	$2(2I_x)^{3/2}(2I_y)^{1/2}$
5	1220	normal	(-1, 2)	(2, -2)	(1, -1)	$2(2I_x)(2I_y)$	$4(2I_x)^{3/2}(2I_y)^{1/2}$
5	1400	normal	(-3, 0)	(4, 0)		$2(2I_x)^2$	
5	2102	normal	(1, -2)	(0, 2)		$4(2I_x)(2I_y)$	
5	2111	normal	(1, 0)	(0, 0)	(-1, 1)	$4(2I_x)(2I_y)$	$2(2I_x)^{3/2}(2I_y)^{1/2}$
5	2120	normal	(1, 2)	(0, -2)	(-1, -1)	$4(2I_x)(2I_y)$	$4(2I_x)^{3/2}(2I_y)^{1/2}$
5	2300	normal	(-1, 0)	(2, 0)		$4(2I_x)^2$	
5	3002	normal	(3, -2)	(-2, 2)		$6(2I_x)(2I_y)$	
5	3011	normal	(3, 0)	(-2, 0)	(-3, 1)	$6(2I_x)(2I_y)$	$2(2I_x)^{3/2}(2I_y)^{1/2}$
5	3020	normal	(3, 2)	(-2, -2)	(-3, -1)	$6(2I_x)(2I_y)$	$4(2I_x)^{3/2}(2I_y)^{1/2}$
5	3200	normal	(1, 0)	(0, 0)		$6(2I_x)^2$	
5	4100	normal	(3, 0)	(-2, 0)		$8(2I_x)^2$	
5	5000	normal	(5, 0)	(-4, 0)		$10(2I_x)^2$	
5	0014	skew	(0, -3)		(0, 4)		$2(2I_y)^2$
5	0023	skew	(0, -1)		(0, 2)		$4(2I_y)^2$

n	jklm	type	resonance	H-line	V-line	Amplitude H	Amplitude V
5	0032	skew	(0, 1)		(0, 0)		$6(2I_y)^2$
5	0041	skew	(0, 3)		(0, -2)		$8(2I_y)^2$
5	0050	skew	(0, 5)		(0, -4)		$10(2I_y)^2$
5	0212	skew	(-2, -1)		(2, 2)		$2(2I_x)(2I_y)$
5	0221	skew	(-2, 1)		(2, 0)		$4(2I_x)(2I_y)$
5	0230	skew	(-2, 3)		(2, -2)		$6(2I_x)(2I_y)$
5	0410	skew	(-4, 1)		(4, 0)		$2(2I_x)^2$
5	1103	skew	(0, -3)	(1, 3)		$2(2I_x)^{1/2}(2I_y)^{3/2}$	
5	1112	skew	(0, -1)	(1, 1)	(0, 2)	$2(2I_x)^{1/2}(2I_y)^{3/2}$	$2(2I_x)(2I_y)$
5	1121	skew	(0, 1)	(1, -1)	(0, 0)	$2(2I_x)^{1/2}(2I_y)^{3/2}$	$4(2I_x)(2I_y)$
5	1130	skew	(0, 3)	(1, -3)	(0, -2)	$2(2I_x)^{1/2}(2I_y)^{3/2}$	$6(2I_x)(2I_y)$
5	1301	skew	(-2, -1)	(3, 1)		$2(2I_x)^{3/2}(2I_y)^{1/2}$	
5	1310	skew	(-2, 1)	(3, -1)	(2, 0)	$2(2I_x)^{3/2}(2I_y)^{1/2}$	$2(2I_x)^2$
5	2003	skew	(2, -3)	(-1, 3)		$4(2I_x)^{1/2}(2I_y)^{3/2}$	
5	2012	skew	(2, -1)	(-1, 1)	(-2, 2)	$4(2I_x)^{1/2}(2I_y)^{3/2}$	$2(2I_x)(2I_y)$
5	2021	skew	(2, 1)	(-1, -1)	(-2, 0)	$4(2I_x)^{1/2}(2I_y)^{3/2}$	$4(2I_x)(2I_y)$
5	2030	skew	(2, 3)	(-1, -3)	(-2, -2)	$4(2I_x)^{1/2}(2I_y)^{3/2}$	$6(2I_x)(2I_y)$
5	2201	skew	(0, -1)	(1, 1)		$4(2I_x)^{3/2}(2I_y)^{1/2}$	
5	2210	skew	(0, 1)	(1, -1)	(0, 0)	$4(2I_x)^{3/2}(2I_y)^{1/2}$	$2(2I_x)^2$
5	3101	skew	(2, -1)	(-1, 1)		$6(2I_x)^{3/2}(2I_y)^{1/2}$	
5	3110	skew	(2, 1)	(-1, -1)	(-2, 0)	$6(2I_x)^{3/2}(2I_y)^{1/2}$	$2(2I_x)^2$
5	4001	skew	(4, -1)	(-3, 1)		$8(2I_x)^{3/2}(2I_y)^{1/2}$	
5	4010	skew	(4, 1)	(-3, -1)	(-4, 0)	$8(2I_x)^{3/2}(2I_y)^{1/2}$	$2(2I_x)^2$
6	0015	normal	(0, -4)		(0, 5)		$2(2I_y)^{5/2}$
6	0024	normal	(0, -2)		(0, 3)		$4(2I_y)^{5/2}$
6	0042	normal	(0, 2)		(0, -1)		$8(2I_y)^{5/2}$
6	0051	normal	(0, 4)		(0, -3)		$10(2I_y)^{5/2}$
6	0060	normal	(0, 6)		(0, -5)		$12(2I_y)^{5/2}$
6	0213	normal	(-2, -2)		(2, 3)		$2(2I_x)(2I_y)^{3/2}$

D

n	jklm	type	resonance	H-line	V-line	Amplitude H	Amplitude V
6	0222	normal	(-2, 0)		(2, 1)		$4(2I_x)(2I_y)^{3/2}$
6	0231	normal	(-2, 2)		(2, -1)		$6(2I_x)(2I_y)^{3/2}$
6	0240	normal	(-2, 4)		(2, -3)		$8(2I_x)(2I_y)^{3/2}$
6	0411	normal	(-4, 0)		(4, 1)		$2(2I_x)^2(2I_y)^{1/2}$
6	0420	normal	(-4, 2)		(4, -1)		$4(2I_x)^2(2I_y)^{1/2}$
6	1104	normal	(0, -4)	(1, 4)		$2(2I_x)^{1/2}(2I_y)^2$	
6	1113	normal	(0, -2)	(1, 2)	(0, 3)	$2(2I_x)^{1/2}(2I_y)^2$	$2(2I_x)(2I_y)^{3/2}$
6	1131	normal	(0, 2)	(1, -2)	(0, -1)	$2(2I_x)^{1/2}(2I_y)^2$	$6(2I_x)(2I_y)^{3/2}$
6	1140	normal	(0, 4)	(1, -4)	(0, -3)	$2(2I_x)^{1/2}(2I_y)^2$	$8(2I_x)(2I_y)^{3/2}$
6	1302	normal	(-2, -2)	(3, 2)		$2(2I_x)^{3/2}(2I_y)$	
6	1311	normal	(-2, 0)	(3, 0)	(2, 1)	$2(2I_x)^{3/2}(2I_y)$	$2(2I_x)^2(2I_y)^{1/2}$
6	1320	normal	(-2, 2)	(3, -2)	(2, -1)	$2(2I_x)^{3/2}(2I_y)$	$4(2I_x)^2(2I_y)^{1/2}$
6	1500	normal	(-4, 0)	(5, 0)		$2(2I_x)^{5/2}$	
6	2004	normal	(2, -4)	(-1, 4)		$4(2I_x)^{1/2}(2I_y)^2$	
6	2013	normal	(2, -2)	(-1, 2)	(-2, 3)	$4(2I_x)^{1/2}(2I_y)^2$	$2(2I_x)(2I_y)^{3/2}$
6	2022	normal	(2, 0)	(-1, 0)	(-2, 1)	$4(2I_x)^{1/2}(2I_y)^2$	$4(2I_x)(2I_y)^{3/2}$
6	2031	normal	(2, 2)	(-1, -2)	(-2, -1)	$4(2I_x)^{1/2}(2I_y)^2$	$6(2I_x)(2I_y)^{3/2}$
6	2040	normal	(2, 4)	(-1, -4)	(-2, -3)	$4(2I_x)^{1/2}(2I_y)^2$	$8(2I_x)(2I_y)^{3/2}$
6	2202	normal	(0, -2)	(1, 2)		$4(2I_x)^{3/2}(2I_y)$	
6	2220	normal	(0, 2)	(1, -2)	(0, -1)	$4(2I_x)^{3/2}(2I_y)$	$4(2I_x)^2(2I_y)^{1/2}$
6	2400	normal	(-2, 0)	(3, 0)		$4(2I_x)^{5/2}$	
6	3102	normal	(2, -2)	(-1, 2)		$6(2I_x)^{3/2}(2I_y)$	
6	3111	normal	(2, 0)	(-1, 0)	(-2, 1)	$6(2I_x)^{3/2}(2I_y)$	$2(2I_x)^2(2I_y)^{1/2}$
6	3120	normal	(2, 2)	(-1, -2)	(-2, -1)	$6(2I_x)^{3/2}(2I_y)$	$4(2I_x)^2(2I_y)^{1/2}$
6	4002	normal	(4, -2)	(-3, 2)		$8(2I_x)^{3/2}(2I_y)$	
6	4011	normal	(4, 0)	(-3, 0)	(-4, 1)	$8(2I_x)^{3/2}(2I_y)$	$2(2I_x)^2(2I_y)^{1/2}$
6	4020	normal	(4, 2)	(-3, -2)	(-4, -1)	$8(2I_x)^{3/2}(2I_y)$	$4(2I_x)^2(2I_y)^{1/2}$
6	4200	normal	(2, 0)	(-1, 0)		$8(2I_x)^{5/2}$	
6	5100	normal	(4, 0)	(-3, 0)		$10(2I_x)^{5/2}$	

n	jklm	type	resonance	H-line	V-line	Amplitude H	Amplitude V
6	6000	normal	(6, 0)	(-5, 0)		$12(2I_x)^{5/2}$	
6	0114	skew	(-1, -3)		(1, 4)		$2(2I_x)^{1/2}(2I_y)^2$
6	0123	skew	(-1, -1)		(1, 2)		$4(2I_x)^{1/2}(2I_y)^2$
6	0132	skew	(-1, 1)		(1, 0)		$6(2I_x)^{1/2}(2I_y)^2$
6	0141	skew	(-1, 3)		(1, -2)		$8(2I_x)^{1/2}(2I_y)^2$
6	0150	skew	(-1, 5)		(1, -4)		$10(2I_x)^{1/2}(2I_y)^2$
6	0312	skew	(-3, -1)		(3, 2)		$2(2I_x)^{3/2}(2I_y)$
6	0321	skew	(-3, 1)		(3, 0)		$4(2I_x)^{3/2}(2I_y)$
6	0330	skew	(-3, 3)		(3, -2)		$6(2I_x)^{3/2}(2I_y)$
6	0510	skew	(-5, 1)		(5, 0)		$2(2I_x)^{5/2}$
6	1005	skew	(1, -5)	(0, 5)		$2(2I_y)^{5/2}$	
6	1014	skew	(1, -3)	(0, 3)	(-1, 4)	$2(2I_y)^{5/2}$	$2(2I_x)^{1/2}(2I_y)^2$
6	1023	skew	(1, -1)	(0, 1)	(-1, 2)	$2(2I_y)^{5/2}$	$4(2I_x)^{1/2}(2I_y)^2$
6	1032	skew	(1, 1)	(0, -1)	(-1, 0)	$2(2I_y)^{5/2}$	$6(2I_x)^{1/2}(2I_y)^2$
6	1041	skew	(1, 3)	(0, -3)	(-1, -2)	$2(2I_y)^{5/2}$	$8(2I_x)^{1/2}(2I_y)^2$
6	1050	skew	(1, 5)	(0, -5)	(-1, -4)	$2(2I_y)^{5/2}$	$10(2I_x)^{1/2}(2I_y)^2$
6	1203	skew	(-1, -3)	(2, 3)		$2(2I_x)(2I_y)^{3/2}$	
6	1212	skew	(-1, -1)	(2, 1)	(1, 2)	$2(2I_x)(2I_y)^{3/2}$	$2(2I_x)^{3/2}(2I_y)$
6	1221	skew	(-1, 1)	(2, -1)	(1, 0)	$2(2I_x)(2I_y)^{3/2}$	$4(2I_x)^{3/2}(2I_y)$
6	1230	skew	(-1, 3)	(2, -3)	(1, -2)	$2(2I_x)(2I_y)^{3/2}$	$6(2I_x)^{3/2}(2I_y)$
6	1401	skew	(-3, -1)	(4, 1)		$2(2I_x)^2(2I_y)^{1/2}$	
6	1410	skew	(-3, 1)	(4, -1)	(3, 0)	$2(2I_x)^2(2I_y)^{1/2}$	$2(2I_x)^{5/2}$
6	2103	skew	(1, -3)	(0, 3)		$4(2I_x)(2I_y)^{3/2}$	
6	2112	skew	(1, -1)	(0, 1)	(-1, 2)	$4(2I_x)(2I_y)^{3/2}$	$2(2I_x)^{3/2}(2I_y)$
6	2121	skew	(1, 1)	(0, -1)	(-1, 0)	$4(2I_x)(2I_y)^{3/2}$	$4(2I_x)^{3/2}(2I_y)$
6	2130	skew	(1, 3)	(0, -3)	(-1, -2)	$4(2I_x)(2I_y)^{3/2}$	$6(2I_x)^{3/2}(2I_y)$
6	2301	skew	(-1, -1)	(2, 1)		$4(2I_x)^2(2I_y)^{1/2}$	
6	2310	skew	(-1, 1)	(2, -1)	(1, 0)	$4(2I_x)^2(2I_y)^{1/2}$	$2(2I_x)^{5/2}$
6	3003	skew	(3, -3)	(-2, 3)		$6(2I_x)(2I_y)^{3/2}$	

D

n	jklm	type	resonance	H-line	V-line	Amplitude H	Amplitude V
6	3012	skew	(3, -1)	(-2, 1)	(-3, 2)	$6(2I_x)(2I_y)^{3/2}$	$2(2I_x)^{3/2}(2I_y)$
6	3021	skew	(3, 1)	(-2, -1)	(-3, 0)	$6(2I_x)(2I_y)^{3/2}$	$4(2I_x)^{3/2}(2I_y)$
6	3030	skew	(3, 3)	(-2, -3)	(-3, -2)	$6(2I_x)(2I_y)^{3/2}$	$6(2I_x)^{3/2}(2I_y)$
6	3201	skew	(1, -1)	(0, 1)		$6(2I_x)^2(2I_y)^{1/2}$	
6	3210	skew	(1, 1)	(0, -1)	(-1, 0)	$6(2I_x)^2(2I_y)^{1/2}$	$2(2I_x)^{5/2}$
6	4101	skew	(3, -1)	(-2, 1)		$8(2I_x)^2(2I_y)^{1/2}$	
6	4110	skew	(3, 1)	(-2, -1)	(-3, 0)	$8(2I_x)^2(2I_y)^{1/2}$	$2(2I_x)^{5/2}$
6	5001	skew	(5, -1)	(-4, 1)		$10(2I_x)^2(2I_y)^{1/2}$	
6	5010	skew	(5, 1)	(-4, -1)	(-5, 0)	$10(2I_x)^2(2I_y)^{1/2}$	$2(2I_x)^{5/2}$

D

Bibliography

[1] *CERN Resources Website*. URL: https://home.cern/resources (visited on 10/02/2023).

[2] Joschua Dilly. “Corrections of High-Order Nonlinear Errors in the LHC and HL-LHC Beam Optics”. To Be Submitted. Humboldt University of Berlin, 2022.

[3] Rob Wolf. *Engineering Specification: Field Error Naming Conventions for LHC Magnets*. Tech. rep. LHC-M-ES-001.00. CERN, Oct. 2001. URL: https://lhc-div-mms.web.cern.ch/lhc-div-mms/tests/MAG/FiDeL/Documentation/lhc-m-es-0001-30-00.pdf (visited on 02/11/2019).

[4] Keintzel Jacqueline. “Beam Optics Design, Measurement and Correction Strategies for Circular Colliders at the Energy and Luminosity Frontier”. en. PhD thesis.

[5] Rogelio Tomás. “Direct Measurement of Resonance Driving Terms in the Super Proton Synchrotron (SPS) of CERN Using Beam Position Monitors”. PhD Thesis. 2003. URL: http://cds.cern.ch/record/615164 (visited on 03/07/2018).

[6] Andrea Franchi. “Studies and Measurements of Linear Coupling and Nonlinearities in Hadron Circular Accelerators”. Doctoral Thesis. Johann Wolfgang Goethe-Universität, Sept. 2006. URL: https://publikationen.ub.uni-frankfurt.de/frontdoor/index/index/year/2006/docId/2270 (visited on 01/19/2018).

[7] E. D Courant and H. S Snyder. “Theory of the Alternating-Gradient Synchrotron”. In: *Annals of Physics* 3.1 (Jan. 1958), pp. 1–48. DOI: 10.1016/0003-4916(58)90012-5. URL: http://www.sciencedirect.com/science/article/pii/0003491658900125 (visited on 05/09/2019).

[8] S. Y. Lee. *Accelerator Physics*. Second. Hackensack, N.J: World Scientific, 2004.

[9] A J Dragt. “An Overview of Lie Methods for Accelerator Physics”. en. In: *Proceedings of PAC*. Pasadena, CA USA: JACoW, 2013.

[10] Ghislain J Roy. “Analysis of the optics of the Final Focus Test Beam using Lie algebra based techniques”. en. PhD thesis. 1992.

[11] Etienne Forest. *Beam dynamics: a new attitude and framework*. en. The physics and technology of particle and photon beams 8. Amsterdam: Harwood Academic, 1998.

[12] Félix Simon Carlier. “A Nonlinear Future: Measurements and Corrections of Nonlinear Beam Dynamics Using Forced Transverse Oscillations”. ISBN: 9789464022148. PhD Thesis. 2020. URL: http://cds.cern.ch/record/2715765/.

[13] Werner Herr. *Mathematical and Numerical Methods for Non-linear Beam Dynamics*. Tech. rep. arXiv: 2006.09052. CERN Accelerator School, 2018. URL: http://arxiv.org/abs/2006.09052 (visited on 07/23/2020).

[14] Félix Soubelet. “Local Interaction Region Coupling Correction for the LHC”. PhD thesis. Sept. 2023. URL: https://cds.cern.ch/record/2891759.

[15] Joschua Dilly and Mael Le Garrec. *On the derivation of Amplitude Detuning and Chromaticity Formulas for Particle Accelerators*. en. arXiv:2301.09132 [physics]. Jan. 2023. URL: http://arxiv.org/abs/2301.09132 (visited on 01/24/2023).

[16] Jacqueline Keintzel et al. “Second-Order Dispersion Measurement in LHC”. In: *IPAC’19*. Melbourne, Australia, 2019, MOPMP027. DOI: 10.18429/JACoW-IPAC2019-MOPMP027.

[17] R. Bartolini and F. Schmidt. “Normal Form via Tracking or Beam Data”. In: *Part. Accel.* 59.LHC-Project-Report-132 (1997), pp. 93–106.

[18] M. Wendt. "BPM Systems: A Brief Introduction to Beam Position Monitoring". In: *ArXiv200514081 Phys.* (May 2020). arXiv: 2005.14081. URL: http://arxiv.org/abs/2005.14081 (visited on 09/01/2021).

[19] A. Nosych. *Geometrical Non-Linearity Correction Procedure Of LHC Beam Position Monitors.* 2014. URL: https://edms.cern.ch/document/1342295/1.

[20] R. Miyamoto et al. "Parametrization of the driven betatron oscillation". en. In: *Physical Review Special Topics - Accelerators and Beams* 11.8 (Aug. 2008), p. 084002. DOI: 10.1103/PhysRevSTAB.11.084002. URL: https://link.aps.org/doi/10.1103/PhysRevSTAB.11.084002.

[21] Javier Serrano and Matthieu Cattin. *The LHC AC Dipole system: an introduction.* en. 2010.

[22] Ewen Hamish Maclean et al. *Commissioning of the nonlinear chromaticity at injection for LHC Run II.* eng. Accelerators & Technology Sector Note 2016-0013. Issue: 2016-0013. 2016. URL: https://cds.cern.ch/record/2121333.

[23] M. Le Garrec. *Non-linear Chromaticity GUI.* Oct. 2022. URL: https://gitlab.cern.ch/mlegarre/nl-chroma-gui.

[24] E H Maclean et al. "Non-linear Chromaticity Studies of the LHC at Injection". en. In: *Proc. IPAC'11.* WEPC078. San Sebastian, Spain, Sep. 2011: JACoW Publishing, Geneva, Switzerland, 2011, pp. 2199–2201. URL: https://jacow.org/IPAC2011/papers/WEPC078.pdf.

[25] Ewen Hamish Maclean, Felix Simon Carlier, and Jaime Coello de Portugal. "Commissioning of Non-linear Optics in the LHC at Injection Energy". In: *Proc. IPAC.* Busan, Korea, 2016, p. 4. DOI: 10.18429/JACoW-IPAC2016-THPMR039. URL: https://cds.cern.ch/record/2207446.

[26] Ewen Hamish Maclean et al. "Measurement of Nonlinear Observables in the Large Hadron Collider Using Kicked Beams". In: *Phys. Rev. ST Accel. Beams* 17.8 (Aug. 2014), p. 081002. DOI: 10.1103/PhysRevSTAB.17.081002. URL: https://link.aps.org/doi/10.1103/PhysRevSTAB.17.081002 (visited on 03/07/2018).

[27] Ewen Hamish Maclean et al. “Measurement of nonlinear observables in the Large Hadron Collider using kicked beams”. In: *Physical Review Special Topics - Accelerators and Beams* 17.8 (Aug. 2014). Number: 8, p. 081002. DOI: 10.1103/PhysRevSTAB.17.081002. URL: https://link.aps.org/doi/10.1103/PhysRevSTAB.17.081002 (visited on 03/07/2018).

[28] M. Gasior and R. Jones. *The Principle and First Results of Betatron Tune Measurement by Direct Diode Detection.* 2005. URL: http://cds.cern.ch/record/883298.

[29] A. Boccardi et al. *First Results from the LHC BBQ Tune and Chromaticity Systems.* 2009. URL: http://cds.cern.ch/record/1156349/.

[30] P. Hagen et al. *Wise: An adaptive simulation of the LHC optics.* Tech. rep. 2006. URL: https://cds.cern.ch/record/977794/files/lhc-project-report-971.pdf.

[31] Helmut Wiedemann. *Particle accelerator physics.* 2nd ed. Berlin ; New York: Springer, 1999.

[32] Tobias Persson et al. “Optics Measurements and Correction Plans for the HL-LHC”. In: *IPAC’21.* ISSN: 2673-5490. Campinas, Brazil: JACOW Publishing, Geneva, Switzerland, Aug. 2021, pp. 2656–2659. DOI: 10.18429/JACoW-IPAC2021-WEPAB026. URL: https://accelconf.web.cern.ch/ipac2021/doi/JACoW-IPAC2021-WEPAB026.html (visited on 11/29/2021).

List of Publications

Journal Publications

Journal Publications (co-author)

Conference Proceedings

Conference Proceedings (co-author)

(1) Tobias Persson et al. "Optics Measurements and Correction Plans for the HL-LHC". in: *IPAC'21*. ISSN: 2673-5490. Campinas, Brazil: JACOW Publishing, Geneva, Switzerland, Aug. 2021, pp. 2656–2659. DOI: 10.18429/JACoW-IPAC2021-WEPAB026. URL: https://accelconf.web.cern.ch/ipac2021/doi/JACoW-IPAC2021-WEPAB026.html (visited on 11/29/2021)

Notes